Non-Analytic Singular Continuations of Complex Analytic Dynamical Systems

a thesis
submitted to the faculty of the graduate school
of the university of Minnesota
by

Brett David Bozyk

in partial fulfillment of the requirements
for the degree of
Master of Science

Advisor: Bruce Peckham

July 2012

Abstract

In this paper we explore an area of dynamical systems that we call non-analytic continuations of analytic maps. These could have many forms, but we are interested in:

$$F_{\beta,c}(z) = z^n + c + \frac{\beta}{\overline{z}^d},$$

where $c, \beta \in \mathbb{C}$, $\overline{z}$ is the complex conjugate of $z \in \mathbb{C}$ or $\hat{\mathbb{C}}$, and $n, d \in \mathbb{N}$. We are particularly interested in the case $c = 0$ with $n = d$. When viewed as a map of the real plane, this "simplest" map decouples into a modulus map, $\mathcal{M}_\beta$, and argument map, $\mathcal{A}_\beta$. Analyzing the modulus map using one-dimensional dynamics yields some interesting results. Among the most significant is the Modulus Trichotomy to where there exists only three possible non escape sets in the dynamic planes, one of which finds the set of bounded orbits empty. This is not possible for complex analytic maps. In the two other cases, most dynamic planes contain a chaotic attractor contained in the interior of the set of bounded orbits. So the set of points which behave chaotically for these maps need not be restricted to the boundary of the set of bounded orbits, which differs from complex analytic maps. Throughout this paper we display some fascinating images and provide descriptions of these complicated topological spaces as we explain these non-analytic continuations.

Acknowledgments

I would like to first thank my advisor, Bruce Peckham, who got me interested in dynamical systems years ago. Since then, he's been more than helpful with his advisement and providing the interesting topic choice for this thesis. Furthermore, I would like to thank him for taking the time out of his schedule to meet almost every week over the course of this study, even weeks when progress was minimal. In addition, I would like to thank Professor John Pastor and Professor Marshall Hampton for serving on my committee, taking the time to read this paper, and hearing the defense. Last but not least, I would like to thank Karli Miller (soon to be Bozyk) for all the encouragement over the course of this study and my entire academic career.

Contents

List of Figures

Below is a list of figures found in this paper to which descriptions can be found on the corresponding page numbers.

1 Introduction

Singular Perturbations have been a popular topic in complex dynamical systems in recent years. These maps could take a variety of forms, but we are interested in the form

$$F_{\beta,c}(z) = z^n + c + \frac{\beta}{\overline{z}^d}, \tag{1}$$

where $c, \beta \in \mathbb{C}$, $\overline{z}$ is the complex conjugate of $z \in \mathbb{C}$ or $\hat{\mathbb{C}}$, and $n, d \in \mathbb{N}$. For the majority of this paper β serves as the primary parameter while c, n, and d serve as secondary or auxiliary parameters. To further simplify the study, we restrict $n \geq 2$ and $n \geq d$ with particular interest to the case where $c = 0$ and $n = d$.

We view $F_{\beta,c}$ as a discrete dynamical system. That is, given a *seed*, z_0, $F_{\beta,c}$ generates the *orbit* $z_0, z_1, z_2, ..., z_n, z_{n+1}, ...$ where $z_k = F_{\beta,c}(z_{k-1}) = F^{(k)}_{\beta,c}(z_0)$. Our aim is to study and classify all possible orbits for $F_{\beta,c}$. But first, let us explain the title non-analytic singular continuations of complex analytic dynamical systems. We start with a complex analytic dynamical system that is "well understood." For (1), this well understood family of functions is defined by $f_c : z \mapsto z^n + c$. Then, f_c serves as a basis for comparison for $F_{\beta,c}$. That is, when $\beta = 0$ we understand the dynamics of $F_{0,c}$ because $F_{0,c} \equiv f_c$. For richer dynamics, we simply allow β to be nonzero and we have continued f_c with a non-analytic family of maps with a pole at the origin, where a pole is any value that is mapped to the point at infinity. Furthermore, $F_{\beta,c}$ leaves the class of polynomial mappings and joins the class of rational maps. What makes $F_{\beta,c}$ particularly interesting is for $\beta = 0$ it is complex analytic, whereas this fails to be true for $\beta \neq 0$. However, when $F_{\beta,c}$ is viewed as a map of the real plane, $\mathbb{R}^2$, $F_{\beta,c}$ is always real rational. It is this reason why the majority of this paper switches between maps of $\mathbb{C}$ and (equivalent) maps of $\mathbb{R}^2$. Moreover, real maps will be denoted R and complex maps will be denoted F, and this change of coordinates is diagrammed below:

$$\begin{array}{ccccc} & \mathbb{C} & \xrightarrow{F} & \mathbb{C} & \\ h & \downarrow & & \downarrow & h \\ & \mathbb{R}^2 & \xrightarrow{R} & \mathbb{R}^2 & \end{array}$$

where $h(x + i \cdot y) = (x, y)$. Since F and R are conjugate, their dynamical properties are the same.

Secondly, the parameters β and c can be viewed as well in $\mathbb{C}$ or $\mathbb{R}^2$ via $\beta = \beta_1 + i \cdot \beta_2 \leftrightarrow (\beta_1, \beta_2)$ and $c = c_1 + i \cdot c_2 \leftrightarrow (c_1, c_2)$. In every case it should be clear by context in which space ($\mathbb{C}$ or $\mathbb{R}^2$) the dynamic variables or parameters live. Also, an abuse of terminology occurs when I say these are maps of the plane. The space we are actually working with is the closure of the plane, or the one point compactification of the plane, $\hat{\mathbb{C}} = \mathbb{C} \cup \{\infty\}$ or $\hat{\mathbb{R}^2} = \mathbb{R}^2 \cup \{\infty\}$; we allow the point at infinity to be a variable in both contexts. Still, we can think of $F_{\beta,c}$ as a map of the plane with an additional point at infinity. For all the maps we consider in this paper, infinity is an attracting fixed point.

The motivation for this paper is based on the topics in [Dr], [Pe1], [Pe2] and the family studied in [De2], [De3], [De4], and [De5] defined as follows:

$$G_{\lambda,c}(z) = z^n + c + \frac{\lambda}{z^d}, \tag{2}$$

where $c, \lambda \in \mathbb{C}$ and $n, d \in \mathbb{N}$ with $n \geq 2$ and $n \geq d$. The maps defined in (2) look very similar to those defined in (1). Both $F_{\beta,c}$ and $G_{\lambda,c}$ have the same "well understood" base function, $z^n + c$. So when $\beta = \lambda = 0$, the maps are equivalent. However, when $\lambda, \beta \neq 0$ the dynamics are no longer the same. Some results hold for both families, while others do not. At various points in this paper we will state these similarities or differences, some of which are minor while others are quite significant. An example of this compares the escape trichotomy proved in [De4] with the modulus trichotomy

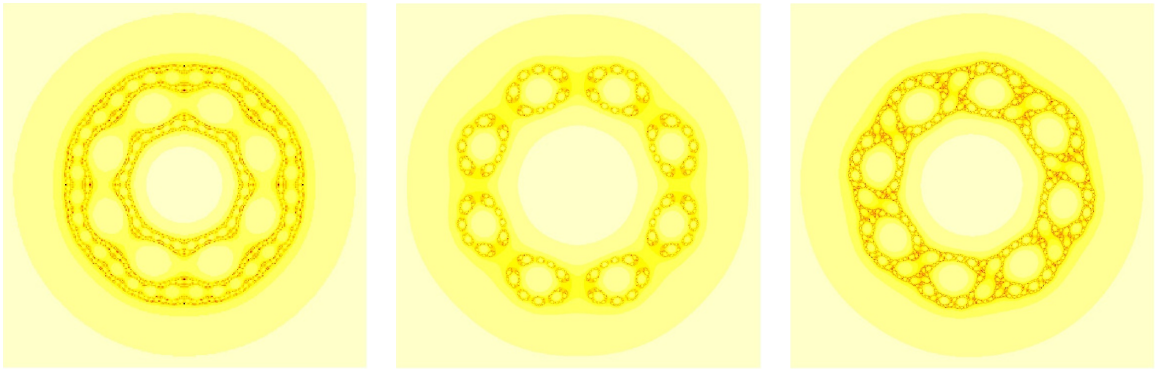

FIGURE 1.1: Examples of the three possible Julia sets for Devaney's trichotomy for $z^4 + \lambda/z^4$ **(Left)** $\lambda = 0.04$ corresponding to the Julia set being a Cantor set of simple closed curves **(Middle)** $\lambda = 0.23$ corresponding to the Julia set being a Cantor set **(Right)** $\lambda = 0.125i$ corresponding to the Julia set being a Sierpinski curve. Given any point in the dynamic plane, its color tells its fate. The darker the color, the longer the point takes to escape. Black points do not escape, but remain bounded.

proved later in this paper. In the escape trichotomy the authors proved in the case where the critical orbit escapes to infinity, there are only three possible Julia sets: a Cantor set, a Cantor set of simple closed curves, and a Sierpinski curve, as displayed in Figure 1.1. We have a similar result for $F_{\beta,0}$, but we also consider the case where the critical orbits are bounded. There are only three possible bounded sets: a closed annulus for the bounded critical orbit and a Cantor set of circles or an empty set for an unbounded critical orbit, displayed in Figure 3.6. For $F_{\beta,c}$ and $G_{\lambda,c}$ they both have a case where a Cantor set of circles is possible. However, they differ in the other cases.

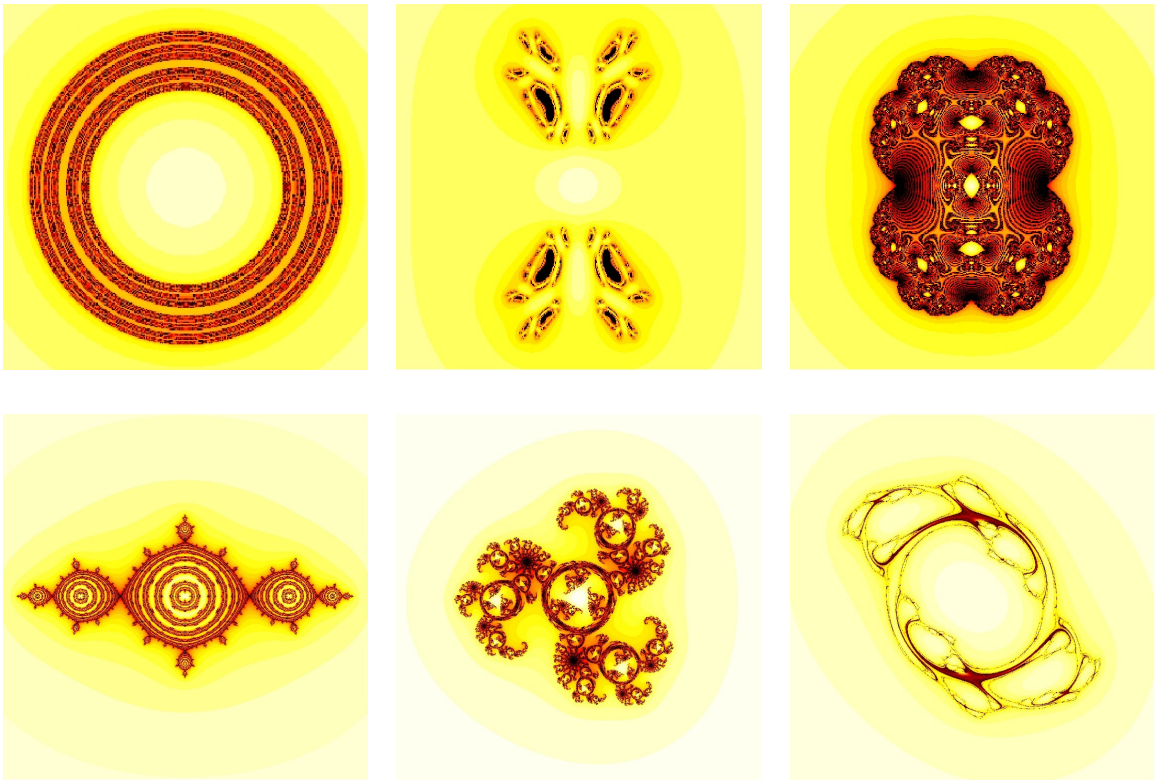

FIGURE 1.2: Examples of various dynamic plane escape sets for $F_{\beta,c}$.

(Top Left) $z^2 + (-0.75 + 0.75i)/\bar{z}^2$ **(Top Middle)** $z^2 + 1 + 0.238/\bar{z}^2$ **(Top Right)** $z^2 + 0.25 - 0.005/\bar{z}^2$ **(Bottom Left)** $z^2 - 1 - 0.001/\bar{z}^2$ **(Bottom Middle)** $z^3 + (0.49 - 0.49i) - 0.001/\bar{z}^3$ **(Bottom Right)** $z^3 + i - (0.6 + 0.1i)/\bar{z}^2$

Here is the same color scheme as described in Figure 1.1.

This paper starts by verifying the fact that $F_{\beta,c}$ satisfies an escape criterion, Theorem 2.1. We then go on to study the simplest case where $n = d$ and $c = 0$. We are able to fully explain the dynamics

for F_β and compare the results to those of (2). We do this by observing that F_β can be reduced to the modulus map, $\mathcal{M}_\beta$, which maps $\mathbb{R}^+$ to $\mathbb{R}^+$. The maps $\mathcal{M}_\beta$ turn out to always be unimodal and results in one-dimensional dynamics help to understand $\mathcal{M}_\beta$, and equivalently $F_{\beta,c}$. Among the theorems proposed is the Modulus Trichotomy (mentioned briefly earlier), which states that there are three possible escape/non-escape sets depending on the orbit of a critical circle. Here there are only three possible sets for the orbits that remain bounded under iteration of F_β: an empty set, a closed annulus, and a Cantor set of geometric circles. Then, a result proved in [deM vSt] allows us to conclude that when the critical orbit is bounded (the closed annulus case above), there exists one of three attractors. It turns out these attractors are always transitive under F_β (Theorem 3.10) and in many cases can behave chaotically. In the cases the attractor is chaotic, it is contained in the interior of the closed annulus. However, a well known result in analytic dynamical systems states that the set of points that behave chaotically is on the boundary of the set of bounded orbits. This is a significant difference from the well studied analytic dynamical systems. We then go on to discuss bifurcation curves and why the case where $n = 2$ is different from $n > 2$. Lastly we finish by proposing some open questions and conjectures for the more general family of functions defined in (1) and provide some numerical observations.

2 An Escape Criterion

Definition: *Escape Criterion* - A condition defined for a iterative map that guarantees all elements that satisfy it necessarily escape, or are attracted to the point at infinity.

$F_{\beta,c}$ has such a criterion with the more general result is proved in Theorem 2.1. Then, proving Lemmas 2.2 and 2.3 we justify an escape criterion for the family of functions defined in (1). Some of the results are proved for functions in the complex plane ($\mathbb{C}$) while others are proved for those in the real plane ($\mathbb{R}^2$). However, through the change of coordinates mentioned in the introduction the result holds true for both spaces.

Theorem 2.1: Let $\beta \in \mathbb{R}^2$ and suppose F_β is a function of the form

$$F_\beta(x,y) = f(x,y) + \frac{\beta}{g(x,y)},$$

where f, g are functions from $\mathbb{R}^2$ to $\mathbb{R}^2$ and two conditions are met:

1. f itself satisfies an escape criterion: there exists some $K > 0$ such that $|(x,y)| > K$ implies $|f(x,y)| > 3|(x,y)|$,
2. there exists some $L > 0$ such that $|(x,y)| > L$ implies $|g(x,y)| > |\beta| / |(x,y)|$.

Then, $|(x,y)| > \max\{K, L\}$ implies $|F_\beta(x,y)| > 2|(x,y)|$ and F_β has an escape criterion.

Proof: Let $|(x,y)| > \max\{K, L\}$. Then by the triangle inequality, the following is true.

$$\begin{aligned} |F_\beta(x,y)| &\geq |f(x,y)| - \frac{|\beta|}{|g(x,y)|} \\ &> 3|(x,y)| - \frac{|\beta|}{|\beta| / |(x,y)|} \\ &= 2|(x,y)| \end{aligned}$$

Therefore, $|(x,y)| > \max\{K, L\}$ implies $|F(x,y)| > 2|(x,y)|$. ■

Next, Lemma 2.2 proves $z^n + c$ satisfies condition 1 of Theorem 2.1.

Lemma 2.2: Given the function $f_c : z \mapsto z^n + c$, $|z| > \max\left\{4^{1/(n-1)}, |c|\right\}$ implies $|f_c(z)| > 3|z|$.

Proof: Let $|z| > \max\left\{4^{1/(n-1)}, |c|\right\}$. With that, $|z| > |c|$ and $|z| > 4^{1/(n-1)}$ which implies $|z|^{n-1} > 4$. Then by the triangle inequality, the following is true:

$$\begin{aligned} |f_c(z)| &\geq |z|^n - |c| \\ &> |z|^n - |z| \\ &= \left(|z|^{n-1} - 1\right)|z| \\ &> (4-1)|z| \\ &= 3|z|. \end{aligned}$$

Therefore, $|z| > \max\left\{4^{1/(n-1)}, |c|\right\}$ implies $|f_c(z)| > 3|z|$. ■

It is important to note that the second condition met in Theorem 2.1 is fairly weak. If any polynomial plays the role of g, then condition 2 is automatically met. We justify this is the case for $F_{\beta,c}$ in Lemma 2.3.

Lemma 2.3: Given $\beta \in \mathbb{C}$ and $d \in \mathbb{N}$, the function $g : z \mapsto \overline{z}^d$, $|z| > |\beta|^{1/(d+1)}$ implies $|g(z)| > |\beta| / |z|$.

Proof: Let $|z| > |\beta|^{1/(d+1)}$. It then follows that $|z|^{d+1} > |\beta|$ and $|g(z)| = \left|\overline{z}^d\right| = |\overline{z}|^d = |z|^d = |z|^{d+1} / |z| > |\beta| / |z|$. Therefore, $|z| > |\beta|^{1/(d+1)}$ implies $|g(z)| > |\beta| / |z|$. ■

Corollary 2.4: $F_{\beta,c}$ as defined in (1), satisfies an escape criterion. More specifically, $|z| > \max\left\{4^{1/(n-1)}, |\beta|^{1/(d+1)}, |c|\right\}$ implies $|F_{\beta,c}(z)| > 2|z|$.

Proof: Lemmas 2.2 and 2.3 justify the two conditions of 2.1. ■

It is worth commenting that this is by no means the best, or most efficient criterion. These values were chosen for simplicity and convenience in the proofs to justify that *some* criterion exists. An escape criterion is extremely useful because all elements that satisfy it can be characterized as having the same dynamics: they are all attracted to the fixed point at infinity. We say the points that satisfy this criterion are in the basin of attraction of ∞, denoted B_β. Furthermore, it allows us to create the standard dynamic and parameter plane images that frequently appear in dynamical systems textbooks and papers. We program the computer to perform the iterative process defined by our map. Our algorithm relies on the fact that we can terminate the iteration process if a given point satisfies an escape criterion because we know from there it will continue to infinity. This gives us the first dichotomy in the dynamic plane: orbits of some points remain bounded, while others don't (those satisfying an escape criterion).

3 The Simplest Case

To gain understanding of $F_{\beta,c}$, it is useful to consider special cases of it. Specifically, we first investigate the case where $n = d$ and $c = 0$ defined in (3).

$$F_\beta(z) = z^n + \frac{\beta}{\bar{z}^n} \tag{3}$$

In (3), $z, \beta \in \mathbb{C}$ with $n \in \mathbb{N}$ and $n \geq 2$. An mentioned in the introduction, it can be useful to view F_β as a map of the real plane as opposed to a map of the complex plane. For easier calculations, we consider z in its polar representation. If $z = re^{i\theta}$ with $r, \theta \in \mathbb{R}$, we have the following relationship.

$$F_\beta\left(re^{i\theta}\right) \leftrightarrow R_\beta \begin{pmatrix} r \\ \theta \end{pmatrix}$$

Throughout this paper we also use rectangular and polar coordinates for parameters. These are represented as $\beta = \beta_1 + \beta_2 i$ and $\beta = |\beta| e^{i\phi}$ respectively, where $\beta_1, \beta_2, |\beta|, \phi \in \mathbb{R}$. Then the relationship $\mathbb{C} \leftrightarrow \mathbb{R}^2$ for β is as follows: $\beta \leftrightarrow (\beta_1, \beta_2) \leftrightarrow (|\beta|, \phi)$. For the remainder of the paper the choice for rectangular or polar coordinates depends on which makes calculations easier.

3.1 Defining R_β

The first result is that the modulus component of R_β decouples from the angular component of R_β. That is, circles in the plane centered at the origin map to circles in the plane centered at the origin. To justify this we need to compute $\left|F_\beta\left(re^{i\theta}\right)\right|$, where $|\cdot|$ is the usual Euclidean norm and $z = re^{i\theta}$.

$$\begin{aligned} F_\beta\left(re^{i\theta}\right) &= \left(re^{i\theta}\right)^n + \frac{\beta}{\left(re^{-i\theta}\right)^n} \\ &= r^n e^{in\theta} + \frac{\beta}{r^n} e^{in\theta} \\ &= \left(r^n + \frac{\beta}{r^n}\right) e^{in\theta} \end{aligned} \tag{4}$$

This implies

$$\left|F_\beta\left(re^{i\theta}\right)\right| = \left|\left(r^n + \frac{\beta}{r^n}\right) e^{in\theta}\right| = \left|r^n + \frac{\beta}{r^n}\right|.$$

The fact that $\left|F_\beta\left(re^{i\theta}\right)\right|$ does not depend on θ justifies the fact that circles centered at the origin map to circles centered at the origin. Now let $\beta = \beta_1 + i\beta_2$ where $\beta_1, \beta_2 \in \mathbb{R}$ and we get the following.

$$\begin{aligned}
\left|F_\beta\left(re^{i\theta}\right)\right| &= \left|r^n + \frac{\beta_1 + i\beta_2}{r^n}\right| \\
&= \left|\left(r^n + \frac{\beta_1}{r^n}\right) + \left(\frac{\beta_2}{r^n}\right)i\right| \\
&= \sqrt{\left(r^n + \frac{\beta_1}{r^n}\right)^2 + \left(\frac{\beta_2}{r^n}\right)^2} \\
&= \sqrt{r^{2n} + 2\beta_1 + \frac{\beta_1^2 + \beta_2^2}{r^{2n}}} \equiv \mathcal{M}_\beta(r) \qquad (5)
\end{aligned}$$

The equation defined in (5) describes the modulus component of F_β, which we refer to as $\mathcal{M}_\beta$ from here on out. Again, $\mathcal{M}_\beta$ is independent of the angle of z and purely dependent on r (the modulus of z). Therefore, $\mathcal{M}_\beta$ is a one-dimensional map from $\mathbb{R}^+$ to $\mathbb{R}^+$ that depends on $\beta \in \mathbb{R}^2$.

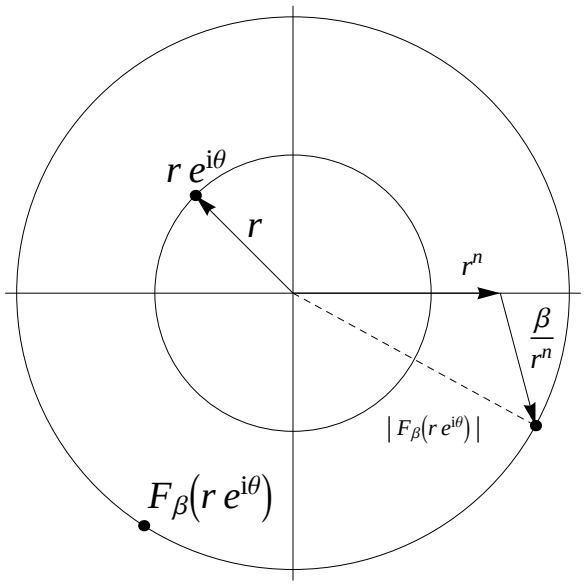

FIGURE 3.1: A general portrayal of how a circle of radius r, centered at the origin, maps to a circle of radius $\left|F_\beta\left(re^{i\theta}\right)\right|$. Furthermore, it shows how a specific point, $re^{i\theta}$, on the circle maps to a new point on the image of the circle. Another interesting property of this map is that every circle maps n to 1 onto the image circle; the initial circle is wrapped n times around the image circle. This observation helps in later proofs in this paper.

The angular component of $F_\beta\left(re^{i\theta}\right)$ can be calculated in a similar fashion, except we find $\arg\left(F_\beta\left(re^{i\theta}\right)\right)$ instead of $\left|F_\beta\left(re^{i\theta}\right)\right|$. Continuing from (4), we can define $\arg\left(F_\beta\left(re^{i\theta}\right)\right)$ as follows.

$$\arg\left(F_\beta\left(re^{i\theta}\right)\right) = \arg\left(r^n + \frac{\beta}{r^n}\right) + n\theta \equiv \mathcal{A}_\beta(r,\theta) \pmod{2\pi}$$

Combining the modulus calculation along with the angular calculation, we can finally define R_β.

$$F_\beta\left(re^{i\theta}\right) \leftrightarrow R_\beta\begin{pmatrix} r \\ \theta \end{pmatrix} = \begin{pmatrix} \mathcal{M}_\beta(r) \\ \mathcal{A}_\beta(r,\theta) \end{pmatrix} = \begin{pmatrix} \sqrt{r^{2n} + 2\beta_1 + \frac{\beta_1^2+\beta_2^2}{r^{2n}}} \\ n\theta + \arg\left(r^n + \frac{\beta}{r^n}\right) \end{pmatrix}$$

Before we proceed, we should emphasize again that $R_\beta : \mathbb{R}^2 \to \mathbb{R}^2$ and every variable or parameter in the definition now lives in $\mathbb{R}$ or $\mathbb{R}^2$. An observation from R_β's definition is that $\mathcal{M}_\beta$ depends only upon r, while $\mathcal{A}_\beta$ depends on both r and θ. Such maps are usually referred to as skew symmetric maps of the plane. Furthermore, since $\mathcal{M}_\beta$ depends only on r, we can analyze the dynamics of $\mathcal{M}_\beta : [0,\infty] \to [0,\infty]$, which will give us valuable insight about the dynamics of F_β and R_β. Note that we are viewing $\mathcal{M}_\beta$ as the closure of the real line, $\mathbb{R} \cup \{\infty\}$. But since r is the modulus of z, we further restrict $\mathcal{M}_\beta$ to the non-negative reals or infinity, $[0,\infty]$. The point is that $\mathcal{M}_\beta$ is a one-dimensional real map, and we have many tools at our disposal to understand the dynamics. In the next sub-section we do just that.

3.2 The Modulus Component

As observed previously, the modulus component, $\mathcal{M}_\beta$, decouples from the angular component. This is true because $\mathcal{M}_\beta$ is a function only of r. This leads to the fact that circles centered at the origin in the plane, map to circles centered at the origin; these circles are invariant under F_β (in $\mathbb{C}$) or R_β (in $\mathbb{R}^2$).

Since $\mathcal{M}_\beta$ is a function of a single variable, r, we need to know how to interpret the behaviors of orbits under $\mathcal{M}_\beta$, and more importantly, how to interpret these behaviors under the full maps, F_β or R_β. The easiest way to visualize the relationship would be to consider a single value in $[0,\infty]$. Call it r_0. We then can study the orbit $r_0, r_1, ...$, where $r_k = \mathcal{M}_\beta(r_{k-1})$. In this context, the orbit is

a sequence of non-negative real numbers or ∞. However, under the maps of the plane, each orbit is a sequence of points on circles centered at the origin with radii $r_0, r_1, r_2, \ldots$. But before we classify the possible orbits of these radii, let us define some notation.

$$\begin{aligned}
\mathcal{M}_\beta^{(k)}(r) &= \overbrace{(\mathcal{M}_\beta \circ \mathcal{M}_\beta \circ \cdots \circ \mathcal{M}_\beta)}^{k\text{-times}}(r) \\
K(\mathcal{M}_\beta) &= \left\{ r \in \mathbb{R} : \mathcal{M}_\beta^{(k)}(r) \not\to \infty \text{ as } k \to \infty \right\} \\
K^c(\mathcal{M}_\beta) &= \left\{ r \in \mathbb{R} : \mathcal{M}_\beta^{(k)}(r) \to \infty \text{ as } k \to \infty \right\} \\
J(\mathcal{M}_\beta) &= \partial K(\mathcal{M}_\beta)
\end{aligned}$$

Even though these sets are defined in the same fashion as the filled Julia set, Julia set, and Fatou set in complex dynamics, we will avoid calling them this. But rather, we will address the set $K(\mathcal{M}_\beta)$ as the set of all r values whose orbits remain bounded under $\mathcal{M}_\beta$, the set $K^c(\mathcal{M}_\beta)$ as the set of all r values whose orbits converge to ∞ under $\mathcal{M}_\beta$, and $J(\mathcal{M}_\beta)$ as the boundary of the set of r values whose orbits remain bounded under $\mathcal{M}_\beta$. Even though the terms filled Julia set, Julia set, and Fatou set may make sense in the context of $\mathcal{M}_\beta$, we will find that it will be a severe abuse of terminology in the context of the full maps of the plane.

The first dichotomy we consider is which orbits of r remain bounded under $\mathcal{M}_\beta$ and which do not. These are the sets $K(\mathcal{M}_\beta)$ and $K^c(\mathcal{M}_\beta)$ respectively. This is a fairly standard approach for such maps. Existing results in one-dimensional dynamics can be applied since $\mathcal{M}_\beta$ is unimodal for all n and β (look ahead to Figure 3.3). Furthermore, the study can be simplified by considering the Schwarzian derivative of $\mathcal{M}_\beta$.

Definition: *Schwarzian derivative* - given a function $P \in C^3$, its Schwarzian derivative is as follows.

$$SP(x) = \frac{P'''(x)}{P'(x)} - \frac{3}{2}\left(\frac{P''(x)}{P'(x)}\right)^2$$

As stated in [De1], the Schwarzian derivative is one of the stranger tools in dynamics. It may also be one of the most important because of the following theorem.

Theorem 3.1: [De1] If $SP(x) < 0$ for all x (in the domain of P) and x_0 is an attracting periodic

point for P, then either there is a critical point of P whose orbit is attracted to the orbit of x_0 or the immediate basin of attraction for x_0 extends to $\pm\infty$.

Unfortunately, the Schwarzian derivative for $\mathcal{M}_\beta$ need not be negative for all $r \in [0, \infty]$. However, we can employ a trick. Let us consider a change of coordinates.

$$\begin{array}{ccccc} & r & \xrightarrow{\mathcal{M}_\beta} & R & \\ h & \downarrow & & \downarrow & h \\ & r^2 & \xrightarrow[\widetilde{\mathcal{M}}_\beta]{} & R^2 & \end{array}$$

In the commutative diagram above, the down arrows are the change of variables defined by $h : r \mapsto r^2$. Also $\widetilde{M}_\beta : s \mapsto s^n + 2\beta_1 + \left(\beta_1^2 + \beta_2^2\right)/s^n$. Since the domain for $\mathcal{M}_\beta$ is the non-negative reals, h is continuous, one-to-one, onto, and has a continuous inverse. It is a homeomorphism. Therefore, any topological property that holds for the "square map", $\widetilde{\mathcal{M}}_\beta$, also hold for the modulus map $\mathcal{M}_\beta$. The reason we introduce this change of coordinates is because even though $\mathcal{M}_\beta$ does not satisfy the hypothesis for Theorem 3.1, it turns out $\widetilde{M}_\beta$ does. To verify this, we consider β in its polar representation. Assume $|\beta| \geq 0$ and $0 \leq \phi < 2\pi$ is the argument of β. Then the following is true.

$$\begin{aligned} \beta_1 &= |\beta| \cos\phi \\ \beta_1^2 + \beta_2^2 &= |\beta|^2 \\ \left(\mathcal{M}(r)\right)^2 = \widetilde{\mathcal{M}}_\beta\left(r^2\right) &= r^{2n} + 2|\beta|\cos\phi + \frac{|\beta|^2}{r^{2n}} \end{aligned} \tag{6}$$

$$\begin{aligned} \widetilde{\mathcal{M}}_\beta(s) &= s^n + 2|\beta|\cos\phi + \frac{|\beta|^2}{s^n} \\ \widetilde{\mathcal{M}}'_\beta(s) &= ns^{n-1} - n\frac{|\beta|^2}{s^{n+1}} \\ \widetilde{\mathcal{M}}''_\beta(s) &= n(n-1)s^{n-1} + n(n+1)\frac{|\beta|^2}{s^{n+2}} \\ \widetilde{\mathcal{M}}'''_\beta(s) &= n(n-1)(n-2)s^{n-2} + n(n+1)(n+2)\frac{|\beta|^2}{s^{n+3}} \end{aligned}$$

$$
\begin{aligned}
S\widetilde{\mathcal{M}}_\beta(s) &= \frac{\widetilde{\mathcal{M}}'''(x)}{\widetilde{\mathcal{M}}'(x)} - \frac{3}{2}\left(\frac{\widetilde{\mathcal{M}}''(x)}{\widetilde{\mathcal{M}}'(x)}\right)^2 \\
&= \frac{\left(1-n^2\right)\left(|\beta|^4 + s^{4n}\right) - 2\left(1+5n^2\right)|\beta|^2 s^{2n}}{\left(\sqrt{2}s\right)^2\left(|\beta|^2 - s^{2n}\right)^2} \qquad (7)
\end{aligned}
$$

We will avoid the cases where $s = 0$ and $s = |\beta|^{1/n}$ because the we know that $\widetilde{\mathcal{M}}_\beta(0)$ is prefixed at infinity and $S\widetilde{\mathcal{M}}_\beta\left(|\beta|^{1/n}\right)$ is undefined. Therefore we can note that $s > 0$, $|\beta| \geq 0$, $n \geq 2$ and it is easy to verify that (7) is negative for all $s \in (0,\infty]\backslash\left\{|\beta|^{1/n}\right\}$. First, the denominator is always non-negative because it is a product of squares. Next, the first term in the numerator is always negative because $1 - n^2$ is always negative and $|\beta|^4 + s^{4n}$ is always positive. Also, the second term in the numerator is always positive as well by inspection. Thus we have something of the form $[(-) - (+)]/(+)$, which is always negative. Therefore, $\widetilde{\mathcal{M}}_\beta$ satisfies Theorem 3.1. We should also state that the immediate basin of attraction for some attracting periodic point cannot extend to $\pm\infty$ because of the escape criterion proved in Corollary 2.4.

Using $\widetilde{\mathcal{M}}_\beta$, let us now solve for the critical points.

$$
\begin{aligned}
\frac{d}{ds}\widetilde{\mathcal{M}}_\beta(s) &= 0 \\
ns^{n-1} - n\frac{\beta_1^2 + \beta_2^2}{s^{n+1}} &= 0 \\
s^{n-1} &= \frac{\beta_1^2 + \beta_2^2}{s^{n+1}} \\
s^{2n} &= \beta_1^2 + \beta_2^2 \\
s &= \left(\beta_1^2 + \beta_2^2\right)^{1/2n}
\end{aligned}
$$

Identifying the fact that $\beta_1^2 + \beta_2^2 = |\beta|^2$, it is true that the critical point for $\widetilde{\mathcal{M}}_\beta$ is $|\beta|^{1/n}$. Then using h^{-1}, we find the critical point for the original modulus map, $\mathcal{M}_\beta$, is $|\beta|^{1/2n}$. Since the domain of $\mathcal{M}_\beta$ and $\widetilde{\mathcal{M}}_\beta$ is the non-negative reals, there is only one critical point. Also note that under the full maps of the plane, this corresponds to a single critical circle.

At this point we will ignore $\widetilde{\mathcal{M}}_\beta$ for the time being. It was only introduced because the topological properties of it are equivalent to those of $\mathcal{M}_\beta$. And, the fate of critical point under $\widetilde{\mathcal{M}}_\beta$ will have

identical fates to critical point under $\mathcal{M}_\beta$. So even though Theorem 3.1 does not apply directly to $\mathcal{M}_\beta$, we can still use the result.

Furthermore, throughout the paper we use $\mathcal{M}_\beta$ where $\beta = \beta_1 + i\beta_2$ or equivalently $\beta = |\beta| (\cos\phi + i \sin\phi)$. The forms are (8) and (9) respectively.

$$\mathcal{M}_\beta(r) = \sqrt{r^{2n} + 2\beta_1 + \frac{\beta_1^2 + \beta_2^2}{r^{2n}}} \tag{8}$$

$$\mathcal{M}_\beta(r) = \sqrt{r^{2n} + 2|\beta| \cos\phi + \frac{|\beta|^2}{r^{2n}}} \tag{9}$$

3.3 The Parameter Plane

Since we verified in the previous sub-section that there exists only one critical point for $\mathcal{M}_\beta$, we can generate the standard images of the dynamic and parameter planes. For complete details on how to program the iteration into the computer, see Algorithms and Codes in the Appendix.

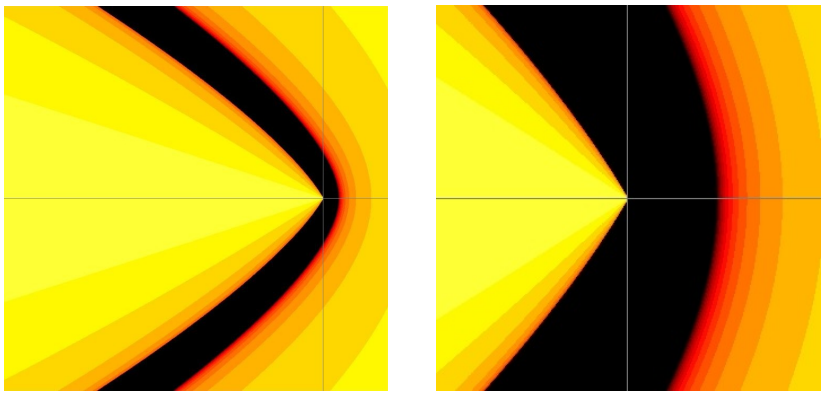

FIGURE 3.2: The β parameter plane for $\mathcal{M}_\beta$, F_β, and R_β. (*Left*) - the parameter plane for $n = 2$ on $[-2.5, 0.5] \times [-1.5, 1.5]\, i$. (*Right*) - a zoomed in window centered at the origin. A $\beta = \beta_1 + i\beta_2$ value chosen inside the black parabola-like region corresponds to a critical circle whose orbit remains bounded under F_β.

Figure 3.2 shows the parameter plane for $n = 2$. There is a parabola-like black region which identifies specific parameter values whose critical circles remain bounded under iteration of F_β. The shading

of the colors is also significant because the darker the color, the longer the the critical circle takes to escape. Furthermore, the parameter planes for $n > 2$ all look similar to those of Figure 3.2. (For $n = 3$ see Figure 3.4.) However, there are significant differences which are addressed in the sub-section Bifurcation Curves and Why the Case $n = 2$ is different.

From generating the images in Figures 3.2 and 3.4, we can immediately observe a few properties of the parameter plane for $\mathcal{M}_\beta$. First, any parameter, β, and its complex conjugate, $\overline{\beta}$, have the same dynamics. Visually, this can be seen by the symmetry about the horizontal axis. This can be confirmed algebraically.

Let $\beta = \beta_1 + i\beta_2$ and $\overline{\beta} = \beta_1 - i\beta_2$ where $\beta_1, \beta_2 \in \mathbb{R}$. Then, the following is true.

$$\mathcal{M}_\beta(r) = \sqrt{r^{2n} + 2\beta_1 + \frac{\beta_1^2 + \beta_2^2}{r^{2n}}} = \sqrt{r^{2n} + 2\beta_1 + \frac{\beta_1^2 + (-\beta_2)^2}{r^{2n}}} = \mathcal{M}_{\overline{\beta}}(r)$$

We know boundedness for $\mathcal{M}_\beta$ corresponds to boundedness for R_β and F_β. So recall that the shading in the parameter plane has significant meaning. Any point in the β parameter plane represents a β value, which has a corresponding critical point (for $\mathcal{M}_\beta$) or a critical circle (for R_β and F_β). A point colored lightly corresponds to a β parameter value whose critical circle escapes quickly under iteration of F_β. The lighter the color, the quicker it escapes, whereas a black point corresponds to critical points/circles that remain bounded under iteration of F_β. Then, another observation is that the color is the lightest along the negative horizontal axis. To justify why this occurs, fix a ray out from the origin at an angle of π, $\beta = |\beta| e^{i\cdot\pi}$ and consider the fate of the critical orbit $|\beta|^{1/2n}$. Using $\mathcal{M}_\beta$ as defined in (9), the following is true.

$$\begin{aligned}
\mathcal{M}_\beta\left(|\beta|^{1/2n}\right) &= \sqrt{\left(|\beta|^{1/2n}\right)^{2n} + 2|\beta|\cos\pi + \frac{|\beta|^2}{\left(|\beta|^{1/2n}\right)^{2n}}} \\
&= \sqrt{|\beta| - 2|\beta| + |\beta|} \\
&= 0
\end{aligned}$$

Since $\mathcal{M}_\beta(0) = \infty$, and infinity is a fixed point, we say that $\mathcal{M}_\beta\left(|\beta|^{1/2n}\right)$ is fixed at infinity after two iterates; it escapes very quickly and this is noticeable since the color along the negative horizontal axis is the lightest. We then can say that every parameter value on the ray defined earlier is in the

same equivalence class, fixed at infinity after two iterates. In addition to that, there seems to be some distinct structure to the β parameter plane. To analyze its structure, we need to study the critical orbit and understand why it escapes or remains bounded.

3.4 The Critical Orbit and the Dynamical Plane

We know that there is significant meaning by following only the orbit of the critical orbit, but in some contexts it can be just as useful looking at the first two iterates of the critical orbit.

$$|\beta|^{1/2n} \to \mathcal{M}_\beta\left(|\beta|^{1/2n}\right) \to \mathcal{M}_\beta^{(2)}\left(|\beta|^{1/2n}\right) \to \cdots$$

From our definition in (9), we can explicitly state the previous expression.

$$|\beta|^{1/2n} \to \sqrt{2\,|\beta|\,(1+\cos\phi)} \to \sqrt{2^n\,|\beta|^n\,(1+\cos\phi)^n + 2\,|\beta|\cos\phi + \frac{|\beta|^2}{2^n\,|\beta|^n\,(1+\cos\phi)^n}} \to \cdots \tag{10}$$

It is interesting to point out that the first iterate of the critical point does not depend on n. In addition, graphical iteration plays a huge role in observing different types of behaviors. (See Figure 3.3.) For any β parameter, $\mathcal{M}_\beta$ is always a unimodal map. It assumes one absolute minimum that occurs at the critical point. It is this fact that makes the dynamics of $\mathcal{M}_\beta$ analogous to the classic family of functions, x^2+c. What situations are possible for x^2+c and how are they similar to $\mathcal{M}_\beta$? From Figure 3.3, we can see for case A that the critical orbit grows monotonically towards infinity, much like $c > 1/4$ for x^2+c. For case B, the graph of $\mathcal{M}_\beta$ is tangent to the reference line, as for $c = 1/4$. For cases C through D the critical orbit remains bounded. Then, in case E the critical orbit is prefixed at the repelling fixed point, as in $c = -2$. And finally, for case F the critical orbit tends to infinity, but it does so in a non-monotonic fashion. It is in this case, analogous to x^2+c (for $c < -2$), to where a Cantor set of points is left behind. The node of $\mathcal{M}_\beta$ breaks through the invariant box (the dashed box in Figure 3.3). It was alluded to earlier that the first two iterates of the critical orbit play a role in the dynamics. We can split up the unbounded critical orbits into two categories:

1. $\mathcal{M}_\beta\left(|\beta|^{1/2n}\right) > |\beta|^{1/2n}$ or
2. $\mathcal{M}_\beta\left(|\beta|^{1/2n}\right) < |\beta|^{1/2n}$.

These correspond to graphs A and F respectively in Figure 3.3. Here the critical orbit converges to ∞ either monotonically (case 1/graph A) or non-monotonically (case 2/ graph F). This dichotomy plays an important role in the modulus trichotomy, stated later in this section. Also for Figure 3.3 $B - E$, an invariant interval is also displayed.

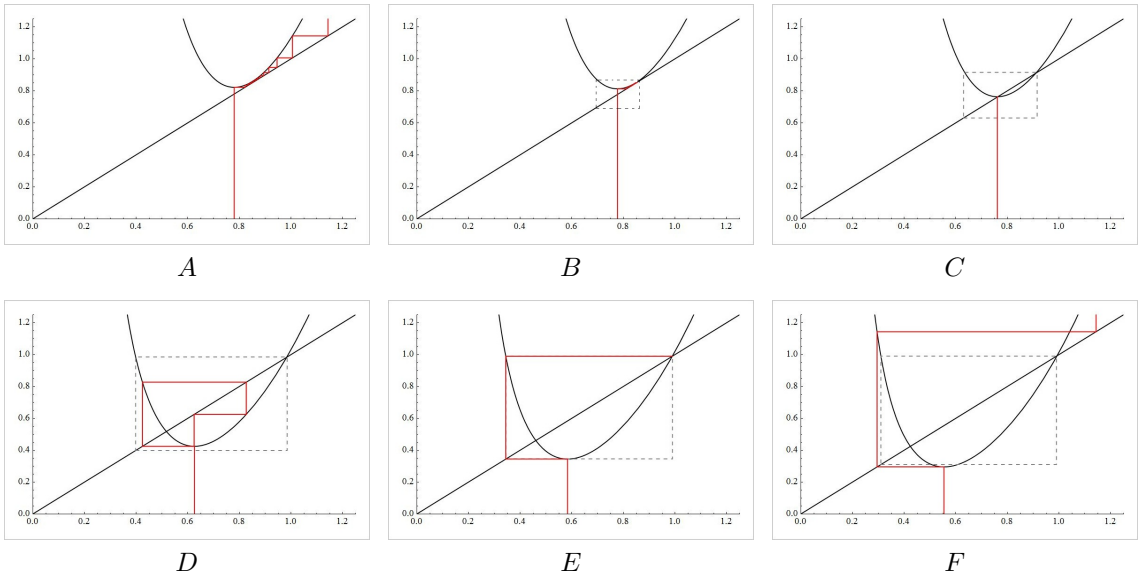

FIGURE 3.3: Displayed here are six possible graphical iterations for $n = 3$ and $\beta = |\beta| e^{i\pi/3}$. That is, the magnitude of the β parameter value varies between six values and the angle of the β parameter value is fixed at $\pi/3$. The β values are chosen to display key bifurcations in the critical orbit. Also, the points $A - F$ are also labeled on the parameter plane in Figure 3.4.

After observing some of the scenarios displayed in Figure 3.3, we would like to know how they are related to the β parameter plane. In Figure 3.4, a ray is fixed at an angle of $\pi/3$ and along that ray are six different points of varying magnitudes. These points correspond to the graphical iterations in Figure 3.3. And from this, we have some valuable insight about the β parameter plane. Clearly if the critical orbit remains bounded, then the β value must lie in the black band in Figure 3.4. Even more, we can explicitly calculate one of the curves contained in the black band, the fixed critical

orbit (displayed in Figure 3.3 C).

$$\begin{aligned}
\mathcal{M}_\beta\left(|\beta|^{1/2n}\right) &= |\beta|^{1/2n} \\
\sqrt{2\,|\beta|\,(1+\cos\phi)} &= |\beta|^{1/2n} \\
2\,|\beta|\,(1+\cos\phi) &= |\beta|^{1/n} \\
2\,(1+\cos\phi) &= |\beta|^{(1-n)/n} \\
[2\,(1+\cos\phi)]^{n/(1-n)} &= |\beta| \qquad (11)
\end{aligned}$$

The equation displayed in (11) is an explicit curve (in polar coordinates) in the β parameter plane that yields β values whose critical point is fixed, like Figure 3.3 C. This curve is displayed in Figure 3.4 for $n = 3$. Furthermore, we can say that any β value chosen on the green curve has equivalent dynamics and this is an example of an equivalence class. We mention these equivalence classes/bifurcation curves later, but we can make some observations by exploring the parameter plane.

Observation 3.1: *Everything Escapes* - all parameter values which yield $\mathcal{M}_\beta(r) > r$ for all $r \geq 0$ produce no orbits that remain bounded. This case is illustrated in Figure 3.3 A. From this observation the set of parameter values which yield bounded orbits is empty, $K(\mathcal{M}_\beta) = \emptyset$. Since $\mathcal{M}_\beta(r) > r$, every seed produces an unbounded strictly monotonic increasing sequence: $r_0 \to r_1 \to r_2 \to \cdots$ where $r_0 < r_1 < r_2 < \cdots$. Obviously if this is the case for all orbits, it is true for the critical orbit; the critical orbit is strictly monotonic increasing. In the β parameter plane, any value chosen to the right of the black band yields this situation and the set of points which remain bounded is empty.

Observation 3.2: *Point of Tangency* - there exists a set of β values, where the graph of $\mathcal{M}_\beta$ is tangent to the reference line, see Figure 3.3 B. Any parameter chosen on the right boundary of the black band in the β parameter plane yields such a graph. Here, critical orbits behave in a strictly monotonic increasing sequence, but unlike Observation 3.1, they are bounded above by the point of tangency/fixed point, $\mathcal{M}_\beta(p) = p$. Therefore if $s_0, s_1, s_2, ...$ is the critical orbit, then $s_0 < s_1 < s_2 < \cdots < p$. Since $\mathcal{M}_\beta$ is a unimodal map opening upward, this is analogous to $c = 1/4$ for the famous map $x^2 + c$.

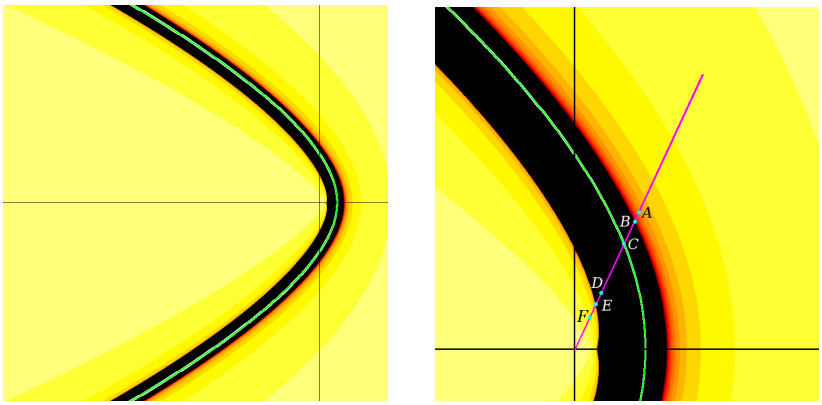

FIGURE 3.4: (*Right*) The β parameter plane for $n = 3$ on $[-2.5, 0.5] \times [-1.5, 1.5]\, i$ and (*Left*) a zoom of the same plane. The letters represent parameter values whose critical orbit are displayed in Figure 3.3. Also, the green curves are traced out by $|\beta| = (2\,(1 + \cos\phi))^{-3/2}$. Any parameter value chosen on this curve corresponds to a critical orbit that is fixed.

OBSERVATION 3.3: *Fixed Critical Point* - there exists an unbounded curve defined by (11) in the parameter plane where the critical orbit is fixed. The fact that this curve is unbounded and is contained in the black band tells us the black band is also an unbounded set.

OBSERVATION 3.4: *Periodic Bifurcation Curves* - much like the the fixed critical point curve in Observation 3.3, there exists curves that yield periodic critical orbits. We will further explain this in the sub-section about bifurcation curves.

OBSERVATION 3.5: *Prefixed Critical Orbit* - there exists a set of parameters which yield graphs of $\mathcal{M}_\beta$ where the critical point is fixed after two iterates. See Figure 3.3 E. Any parameter chosen on the left boundary of the black band in the β parameter plane yields such a graph. Here, the critical orbit is $s_0, s_1, s_2, s_2, ...$ where $s_1 < s_0 < s_2$. This situation is analogous to $c = -2$ for $x^2 + c$.

OBSERVATION 3.6: *Unimodal Breakthrough* - lastly, any β value chosen to the left of the black band yields a graph of $\mathcal{M}_\beta$ whose critical point breaks through an invariant box whose vertices include the points (p_+, p_+) and $\left(\mathcal{M}_\beta^{\text{pre}}(p_+), \mathcal{M}_\beta^{\text{pre}}(p_+)\right)$, where p_+ is the larger of the repelling fixed points and $\mathcal{M}_\beta^{\text{pre}}(p_+)$ is its other preimage. (See Figure 3.3 F). This is analogous to the case where $c < -2$ for $x^2 + c$. Here the critical orbit escapes, but does so non-monotonically.

Since the β parameter plane only tracks the fate of a single (critical) orbit, it is natural to wonder

how the critical orbit plays into other orbits. That is, if we know the fate of the critical orbit, can we say anything about the other possible orbits in the dynamic plane? We address that question next.

From understanding the previous observations, it turns out there exists only three possibilities for the set of bounded points, $K(F_\beta)$, in the dynamic plane: an empty set, a closed annulus, or a Cantor set of geometric circles. In any case, the fate of the critical orbit tells us the structure of $K(F_\beta)$.

Theorem 3.2: *The Modulus Trichotomy*
Let $s_0, s_1, s_2...$ be the orbit of the critical point for $\mathcal{M}_\beta$.

1. If the critical orbit remains bounded, then the set of points which remain bounded is a closed interval for $\mathcal{M}_\beta$, or equivalently a closed annulus for F_β.
2. If the critical orbit tends to infinity and $s_i < s_j$ for all $i < j$, then all orbits for $\mathcal{M}_\beta$ (and equivalently F_β) tend to infinity. That is, $K(\mathcal{M}_\beta) = K(F_\beta)$ is empty.
3. If the critical orbit tends to infinity, but $s_1 < s_0 < s_2$, then $K(\mathcal{M}_\beta)$ is a Cantor set and $K(F_\beta)$ is a Cantor set of geometric circles.

Justifying claim 1: Observe that $\mathcal{M}_\beta$ is a unimodal map opening upward. It is well known that the set of points that remain bounded will be a closed connected set, much like $x^2 + c$ for $-2 \leq c \leq 1/4$. This closed, connected set will have to be a closed connected interval in $\mathbb{R}^+$. Full the full map, F_β, wrapping this set around the origin will yield a closed annulus under F_β. ■

Justifying Claim 2: If the critical orbit tends to infinity in a strictly monotonic sequence, then the same is true for all r in the domain of $\mathcal{M}_\beta$. This stems from the properties explained in Observation 3.1. Next, if all $r \geq 0$ tend to infinity under $\mathcal{M}_\beta$, then all circles of positive radius grow infinitely large under F_β, with a special note that the origin is fixed at infinity after one iterate. Then, no points remain bounded under either $\mathcal{M}_\beta$ or F_β , $K(\mathcal{M}_\beta) = K(F_\beta) = \emptyset$. We remark that this case is not possible for complex analytic dynamical systems. ■

Justifying Claim 3: As mentioned previously, $\mathcal{M}_\beta$ is conjugate to the square map $\widetilde{\mathcal{M}_\beta}$ by the change of variables $h : r \mapsto r^2$. The square map is unimodal and has negative Schwarzian for all non critical points in the domain. Since the critical orbit

tends to infinity non-monotonically, we can conclude that $\widetilde{\mathcal{M}}_\beta$, which is conjugate to $\mathcal{M}_\beta$, satisfies the definition of a horseshoe map defined in [Kr2], which is an extension of [Kr1]. The author later proves that the set of points that remain bounded under any horseshoe map is a Cantor set. Therefore, the set of points which remain bounded under the full map, F_β, is a Cantor set of geometric circles. ■

Figure 3.5 illustrates claim 3 in the Modulus Trichotomy above. Whenever the node of the map pushes through the box formed by the largest fixed point and its other preimage, $\mathcal{M}_\beta$ is a horseshoe map.

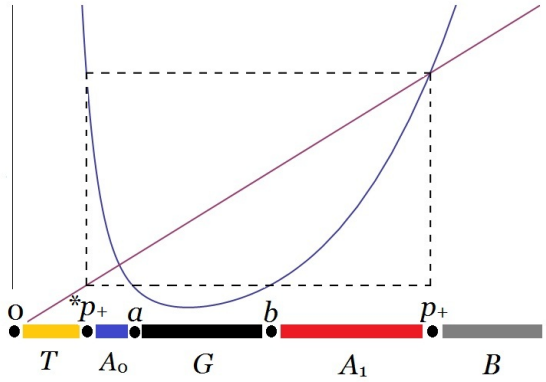

FIGURE 3.5: example of the case where the critical orbit breaks through the invariant box. This also illustrates the basin of attraction, B, the trap door, T, and how G maps into the trap door. Note: $*p_+ \equiv \mathcal{M}_\beta^{\text{pre}}(p_+)$.

The previous theorem plays a huge role in this study because it essentially shows that there are only three possible sets of points which remain bounded under $\mathcal{M}_\beta$: an empty set , a closed interval, or a Cantor set. Equivalently, under F_β, the three possibilities are an empty set (Figure 3.6 Left), a closed annulus (Figure 3.6 Middle), or a Cantor set of geometric circles (Figure 3.6 Right). The drawback in the theorem is that is says nothing about how the bounded points behave. But, we have not used the angular component, $\mathcal{A}_\beta$, of R_β. As soon as we take $\mathcal{A}_\beta$ into account, we will find that chaotic dynamics are not only possible, but inevitable for most maps in case 2 and all maps in case 3 of the modulus trichotomy.

FIGURE 3.6: examples of the three possible sets of bounded orbits: (*Left*) an empty set, (*Middle*) a closed annulus, and (*Right*) a Cantor set of geometric circles.

3.5 Things Get Chaotic

Recall the angular component defined earlier:

$$\mathcal{A}_\beta(r,\theta) \quad = \quad \arg\left(r^n + \frac{\beta}{r^n}\right) + n\theta.$$

It is not important to understand the exact value of $\arg\left(r^n + \beta/r^n\right)$ in $\mathcal{A}_\beta$, but rather that it is some function of r. We will denote this as Ω_β as follows.

$$\mathcal{A}_\beta(r,\theta) = \Omega_\beta(r) + n\theta$$

Now we can make an observation about the nature of how angles change as iteration is performed.

OBSERVATION 3.7: *Angular Iteration* - let $r_0 e^{i\theta_0}$ be an arbitrary seed for F_β. Here $r_0 e^{i\theta_0}$ is the start of the sequence $r_0 e^{i\theta_0}, F_\beta\left(r_0 e^{i\theta_0}\right), F_\beta^{(2)}\left(r_0 e^{i\theta_0}\right), \cdots = r_0 e^{i\theta_0}, r_1 e^{i\theta_1}, r_2 e^{i\theta_2}, \cdots$. That is, the modulus orbit is defined by $r_0, r_1, r_2, \cdots$ and the angle orbit is defined by $\theta_0, \theta_1, \theta_2, \cdots$. Then, the

angle of $F_\beta^{(k)}\left(r_0 e^{i\theta_0}\right)$ can be generalized by the following.

$$\begin{aligned}
\theta_1 &= n\theta_0 + \Omega_\beta(r_0) \\
\theta_2 &= n\left(n\theta_0 + \Omega_\beta(r_0)\right) + \Omega_\beta(r_1) \\
&= n^2\theta_0 + n\Omega_\beta(r_0) + \Omega_\beta(r_1) \\
\theta_3 &= n\left(n^2\theta_0 + n\Omega_\beta(r_0) + \Omega_\beta(r_1)\right) + \Omega_\beta(r_2) \\
&= n^3\theta_0 + n^2\Omega_\beta(r_0) + n\Omega_\beta(r_1) + \Omega_\beta(r_2) \\
&\vdots \\
\theta_k &= n^k\theta_0 + \sum_{i=0}^{k-1} n^i \cdot \Omega_\beta(r_{k-1-i})
\end{aligned} \tag{12}$$

So the angle of the k^{th} iterate can completely be defined in terms of the initial angle (θ_0) and the previous moduli $(r_0, r_1, \cdots, r_{k-1})$. This observation is quite helpful in the next sequence of lemmas.

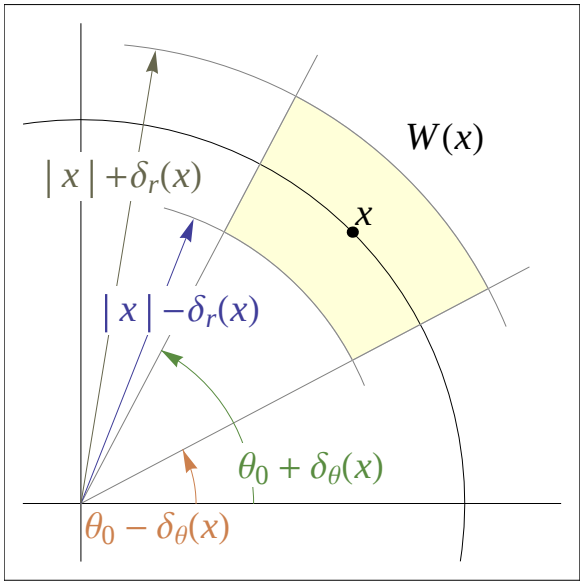

FIGURE 3.7: the chunk of a wedge about $x \in \mathbb{C}$ given $\delta_r(x)$ and $0 < \delta_\theta(x) < \pi$.

Also, we use a special neighborhood about a given point that [De1] calls a *chunk of a wedge*.

DEFINITION: *Chunk of a Wedge* - Given $x = |x| e^{i\theta_x} \in \mathbb{C}$, $0 < \delta_\theta(x) < \pi$ and $\delta_r(x) > 0$, the chunk

of a wedge about x is defined as follows.

$$W_{\delta_r,\delta_\theta}(x) = \left\{re^{i\theta} : |x| - \delta_r(x) \leq r \leq |x| + \delta_r(x), \theta_x - \delta_\theta(x) \leq \theta \leq \theta_x + \delta_\theta(x)\right\}.$$

An illustration of the chunk of a wedge about x is given in Figure 3.7. For the remainder of this paper, we generally consider a fixed $\delta_r(x)$ and $\delta_\theta(x)$. So, to simplify notation we refer to the chunk of a wedge about x as just $W(x)$ instead of $W_{\delta_r,\delta_\theta}(x)$.

LEMMA 3.3: *Chaotic Fixed Circle* - Let $p \in \mathbb{R}^+$ be a fixed point for $\mathcal{M}_\beta$ and $C_p = \left\{pe^{i\theta} : 0 \leq \theta < 2\pi\right\}$. Then, $F_\beta|_{C_p}$ is chaotic.

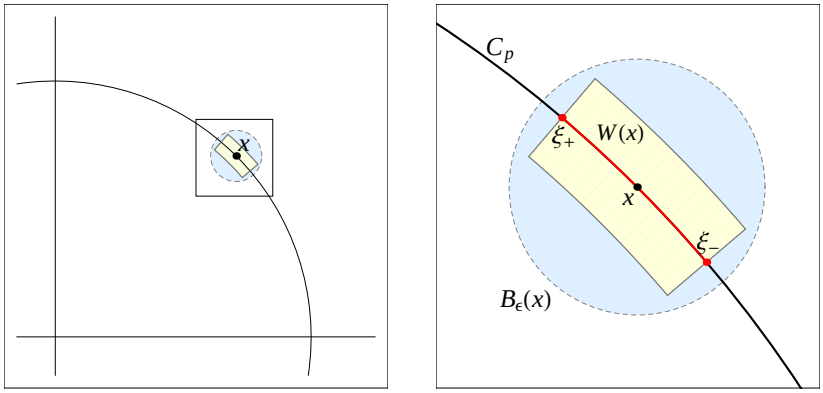

FIGURE 3.8: displays how a chunk of a wedge about any x can fit inside any open ball with radius ϵ about x. For this particular case, C_p is a fixed circle (in magnitude) under F_β and $W(x) \cap C_p$ is represented by the red curve.

PROOF: Since p is a fixed point for $\mathcal{M}_\beta$, then $C_p = \left\{pe^{i\theta} : 0 \leq \theta < 2\pi\right\}$ is a fixed circle (in magnitude) under the full map, F_β. To show $F_\beta|_{C_p}$ is chaotic, consider any $x = pe^{i\theta_x} \in C_p$ and let an arbitrary $\epsilon > 0$ be given. Given the open ball of radius ϵ about x, $B_\epsilon(x)$, we can choose a small enough $\delta_\theta(x)$ and $\delta_r(x)$ such that $W(x) \subset B_\epsilon(x)$. Next, choose $k \in \mathbb{N}$ such that $k > \log_n(\pi/\delta_\theta(x))$. Finally iterate $W(x) \cap C_p$ k times. For an idea of what these sets look like, see Figure 3.8. $W(x) \cap C_p$ is displayed as the

red curve in Figure 3.8 Right and is a closed set. We can also explicitly define this red curve as follows.

$$W(x) \cap C_p = \left\{ pe^{i\theta} : \theta_x - \delta_\theta(x) \leq \theta \leq \theta_x + \delta_\theta(x) \right\}$$

Furthermore, we say the interval of angles for $W(x) \cap C_p$ is $[\xi_-, \xi_+] \subset \mathbb{R}$, where $\xi_\pm = \theta_x \pm \delta_\theta(x)$. We then define the distance between ξ_- and ξ_+ to be the Euclidean distance in $\mathbb{R}$, $|\xi_+ - \xi_-| \in [0, \infty)$. Note that angles under the full map are taken to be modulo 2π, but this need not be true for the interval of angles defined above. Since we have already iterated $k > \log_n(\pi/\delta_\theta(x))$ times, we can find the distance in the angular interval between the k^{th} iterates of the endpoints, ξ_- and ξ_+, denoted $\xi_-^{(k)}$ and $\xi_+^{(k)}$. From (12), $\left|\xi_+^{(k)} - \xi_-^{(k)}\right|$ can be calculated as follows.

$$\begin{aligned}
\left|\xi_+^{(k)} - \xi_-^{(k)}\right| &= \left| \left[n^k(\theta_x + \delta_\theta(x)) + \sum_{i=0}^{k-1} n^i \cdot \Omega_\beta(r_{k-1-i}) \right] \right. \\
&\quad \left. - \left[n^k(\theta_x - \delta_\theta(x)) + \sum_{i=0}^{k-1} n^i \cdot \Omega_\beta(r_{k-1-i}) \right] \right| \\
&= \left| n^k\theta_x + \delta_\theta(x)\, n^k - n^k\theta_x + \delta_\theta(x)\, n^k \right| \\
&= \left| 2\delta_\theta(x)\, n^k \right| \\
&= 2\delta_\theta(x)\, n^k
\end{aligned}$$

Since k was chosen such that $k > \log_n(\pi/\delta_\theta(x))$, the following is true.

$$\begin{aligned}
k &> \log_n(\pi/\delta_\theta(x)) \\
n^k &> \pi/\delta_\theta(x) \\
2\delta_\theta(x)\, n^k &> 2\pi
\end{aligned}$$

Since $\left|\xi_+^{(k)} - \xi_-^{(k)}\right| = 2\delta_\theta(x)\, n^k > 2\pi$ and $W(x) \cap C_p$ is a subset of the fixed circle of magnitude p, it follows that

$$F_\beta^{(k)}(W(x) \cap C_p) = \left\{ pe^{i\theta} : \xi_-^{(k)} \leq \theta \leq \xi_+^{(k)} \right\}. \tag{13}$$

Under the context of F_β, where angles are taken to be modulo 2π, (13) can be redefined as

$$F_\beta^{(k)}\left(W\left(x\right)\cap C_p\right)=\left\{pe^{i\theta}:0\leq\theta<2\pi\right\}=C_p.$$

Therefore, $W\left(x\right)\cap C_p$ is mapped onto C_p after k iterates. With that observation, we can conclude that $F_\beta|_{C_p}$ exhibits dense periodic points and is topologically transitive. First, since $W\left(x\right)\cap C_p$ is mapped onto C_p, there must exist some $pe^{i\psi}\in W\left(x\right)\cap C_p\subset B_\epsilon\left(x\right)$ such that $F_\beta^{(k)}\left(pe^{i\psi}\right)=pe^{i\psi}$ by the intermediate value theorem and we have found a period k point within ϵ of any $x\in C_p$. Periodic points are dense in C_p. Secondly, since $F_\beta^{(k)}\left(W\left(x\right)\cap C_p\right)\supset C_p$ after k iterates, we can find some $z\in W\left(x\right)\cap C_p\subset B_\epsilon\left(x\right)$ such that after k iterates $F_\beta^{(k)}\left(z\right)\in B_\epsilon\left(y\right)$ for any $y\in C_p$. Said differently, z is within ϵ of x and after k iterates is within ϵ of y. $F_\beta|_{C_p}$ is a topologically transitive set. Since topological transitivity and dense periodic points imply chaotic dynamics [Ba], $F_\beta|_{C_p}$ is chaotic. ■

We remark that Lemma 3.3 is similar to the unit circle being chaotic under z^n for any $n\geq 2$, but with a shifted n^{th} map for its angle map. The key component in the proof is that any arbitrarily small interval on any circle will eventually wrap around a circle completely. Lemma 3.3 was special in the sense that we only considered one circle, and it was fixed (in magnitude). We will generalize below, but we need to introduce the idea of a topological attractor.

Definition: *Topological Attractor* [deM vSt] - We say that an invariant set A is a topological attractor, or attractor for short, if its basin $B\left(A\right)=\left\{x,\omega\left(x\right)\subset A\right\}$ satisfies

1. the closure of $B\left(A\right)$ contains intervals;
2. each closed forward invariant subset A' such is strictly contained in A has a smaller basin of attraction: $\text{cl}\left(B\left(A\right)\right)\backslash\text{cl}\left(B\left(A'\right)\right)$ contains intervals.

Attractors for one-dimensional $l-$modal maps have been thoroughly studied in [deM vSt] and since $\mathcal{M}_\beta$ is unimodal ($l=1$), we can use the following result. But, note that the previous definition is

in one-dimension. The analogous two-dimensional attractor would simply be $A \times S^1$, or wrapping the attractor A about the origin.

Theorem 3.4: Under $\mathcal{M}_\beta$, if a parameter value is chosen such that the critical orbit is bounded, then the set of bounded orbits has a topologically transitive attractor $A_{\mathcal{M}_\beta}$ and there is only three possibilities for $A_{\mathcal{M}_\beta}$:

1. $A_{\mathcal{M}_\beta}$ is a periodic orbit,
2. $A_{\mathcal{M}_\beta}$ is a minimal Cantor set, or
3. $A_{\mathcal{M}_\beta}$ is the orbit of a periodic interval.

As a consequence of Theorem 3.4, if the orbit of the critical circle under F_β remains bounded, there exists an analogous attractor, A_{F_β}, that is: (1) a periodic orbit of circles, (2) a minimal Cantor set of circles, or (3) is the orbit of periodic annuli. To illustrate the two-dimensional attractor, consider Lemma 3.3 under the context of the critical point being attracted to the fixed point, p, under $\mathcal{M}_\beta$. We then know an interval of points is attracted to p under $\mathcal{M}_\beta$. This corresponds to the critical circle and the corresponding annulus being attracted to C_p under the full map, F_β. Since we proved C_p was chaotic, F_β would have a *chaotic attractor*.

Since Theorem 3.4 applies to critical points/circles that remain bounded under iteration, we can attempt to explain the dynamics of the black band in the β parameter plane. To generalize Lemma 3.3, we next consider any periodic point of $\mathcal{M}_\beta$ instead of a fixed point. The proof is very similar to Lemma 3.3.

Lemma 3.5: *Chaotic Periodic Circle* - Suppose there exists a period k orbit under $\mathcal{M}_\beta$, $r_0, r_1, \cdots, r_{k-1}, r_0 \cdots$. Then, $F_\beta|_A$ is chaotic, where $A = \bigcup_{i=0}^{k-1} \left\{ r_i e^{i\theta} : 0 \leq \theta < 2\pi \right\}$.

Proof: Let $x = r_0 e^{i\theta_x} \in A$ and $\epsilon > 0$ be given. We know $x \in C_{r_0} = \left\{ r_0 e^{i\theta} : 0 \leq \theta < 2\pi \right\}$ and exactly like Lemma 3.3, we know there exists some $\delta_r(x) > 0$ and $0 < \delta_\theta(x) < \pi$ such that $W(x) \subset B_\epsilon(x)$. Furthermore, choose N such that $N \cdot k > \log_n(\pi/\delta_\theta(x))$. Since $\mathcal{M}_\beta^{(k)}(r_0) = r_0$, by assumption, it is clear that $\mathcal{M}_\beta^{(Nk)}(r_0) = r_0$ as well. From here the argument is the same as Lemma 3.3: define the interval of angles for $W(x) \cap C_{r_0}$ as

$[\xi_-, \xi_+] \subset \mathbb{R}$, where $\xi_\pm = \theta_x \pm \delta_\theta(x)$ and from (12), $\left|\xi_+^{(k)} - \xi_-^{(k)}\right|$ can be calculated as follows.

$$\begin{aligned}
\left|\xi_+^{(k)} - \xi_-^{(k)}\right| &= \left|\left[n^{Nk}\left(\theta_x + \delta_\theta(x)\right) + \sum_{i=0}^{Nk-1} n^i \cdot \Omega_\beta\left(r_{Nk-1-i}\right)\right]\right. \\
&= \\
&\quad \left. - \left[n^{Nk}\left(\theta_x - \delta_\theta(x)\right) + \sum_{i=0}^{Nk-1} n^i \cdot \Omega_\beta\left(r_{Nk-1-i}\right)\right]\right| \\
&= \left|n^{Nk}\theta_x + n^{Nk}\delta_\theta(x) - n^{Nk}\theta_x + n^{Nk}\delta_\theta(x)\right| \\
&= \left|2n^{Nk}\delta_\theta(x)\right| \\
&= 2n^{Nk}\delta_\theta(x)
\end{aligned}$$

Again since we chose $Nk > \log_n\left(\pi/\delta_\theta(x)\right)$, the following is true.

$$\begin{aligned}
Nk &> \log_n\left(\pi/\delta_\theta(x)\right) \\
n^{Nk} &> \pi/\delta_\theta(x) \\
2n^{Nk}\delta_\theta(x) &> 2\pi
\end{aligned}$$

Therefore, $F_\beta^{(Nk)}\left(W(x) \cap C_{r_0}\right) \supset C_{r_0}$and an identical argument as Lemma 3.3 justifies $F_\beta|_{C_{r_0}}$ has dense periodic points and is transitive. Thus, $F_\beta|_{C_{r_0}}$ is chaotic. It then follows that any $C_j \in A$ for $j \in \{r_0, r_1, \cdots, r_{k-1}\}$ can be identified as C_{r_0} above. Therefore, every $C_j \in A$ is chaotic and $F_\beta|_A$ is chaotic as well. ■

Therefore, Lemma 3.5 proves that if the attractor mentioned in Theorem 3.4 is type 1, then $F_\beta|_{A_{F_\beta}}$ is chaotic. That is, almost all bounded orbits will eventually be attracted to a chaotic orbit. This is a significant result, especially since every attractor of this type is contained completely inside $K(F_\beta)$. A well known result for complex analytic dynamical systems states that the set of points that behaves chaotically is $\partial K(F_\beta)$, which is not the case here. However, $\partial K(F_\beta)$ does have either chaotic or eventually chaotic dynamics. Figure 3.9 illustrates this fact for a fixed circle attractor. First, the white circle is the attractor (chaotic fixed circle) for this particular β value and through graphical iteration, we can observe that any seed chosen in the black annulus tends to the chaotic

attractor. With graphical iteration, it is just as easy to see the fates of the inner and outer boundary of the closed annulus. First the magenta/outer boundary is mapped to itself and thus is chaotic by Lemma 3.3. Then, the green/inner boundary is mapped onto the outer boundary and is fixed from there on out. So we say the inner boundary is eventually chaotic. Since Theorem 3.2.1 states closed annuli are the only possibility when the critical orbit is bounded, this is also the case for every β value chosen in the black band of the β parameter plane.

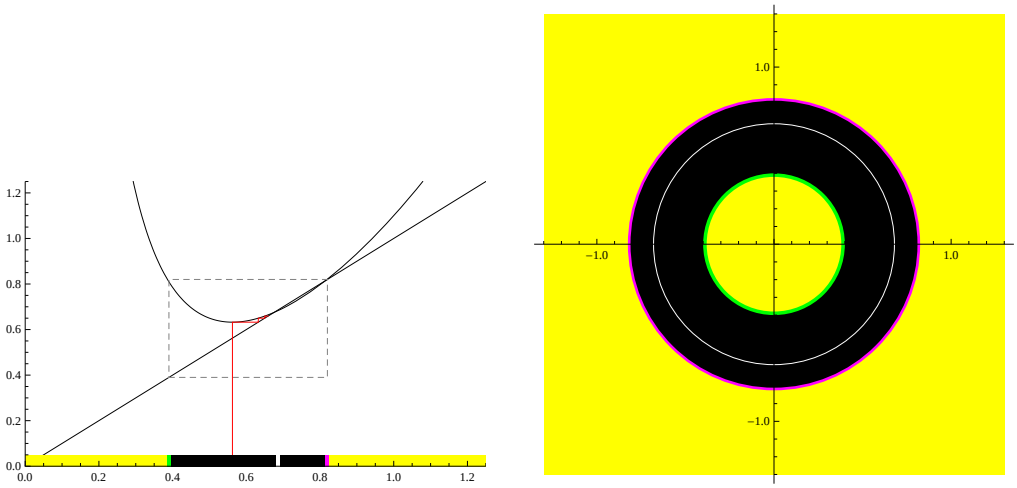

FIGURE 3.9: (*Left*) is graphical iteration of the critical orbit for $\mathcal{M}_{0.1}$ and $n = 2$. (*Right*) is the dynamical plane for $F_{0.1}$. The dynamical plane is equivalent to wrapping the horizontal axis of Left around the origin. The colors help distinguish the different regions.
Yellow - Any seed chosen in the yellow is attracted to the point at infinity, while all other colors remain bounded.
Magenta - A seed chosen on the magenta boundary is fixed (in modulus) on the repelling fixed point/circle.
Green - A seed chosen on the green boundary is prefixed on the repelling fixed point/circle (*magenta*).
White - A seed chosen on the white value is fixed on the attracting fixed point/circle.
Black - Any seed chosen in the black tends to the attracting fixed point/circle (*white*).

With Lemmas 3.3 and 3.5, we can completely understand Case 1 of Theorem 3.4. Now we aim to understand the other two cases. [deM vSt] proved each attractor is transitive for all three cases in Theorem 3.4. Thus, we know that the attractor for $K(\mathcal{M}_\beta)$ is always a topologically transitive set. However, that doesn't necessarily mean the attractor for the full map, F_β, is topologically transitive. However, with a little work we can show that this is the case. We will need the following definition

and Theorem 3.6.

Definition: *Hitting Time Set for $\mathcal{M}_\beta$* - For open sets $X, Y \subset [0, \infty]$, the hitting time set $\mathcal{H}(X, Y) = \left\{k : X \cap \mathcal{M}^{-k}(Y) \neq \emptyset\right\}$.

Theorem 3.6 [Ko]: If $\mathcal{M}_\beta|_A$ is topologically transitive, then for every pair of non-empty open subsets X and Y, the hitting time set $\mathcal{H}(X, Y)$ is infinite.

Lemma 3.7 *Transitivity under $\mathcal{M}_\beta$ Implies Transitivity under F_β* - Suppose β is chosen such that the set of bounded orbits under $\mathcal{M}_\beta$ has a topologically transitive attractor, $A_{\mathcal{M}_\beta}$. Then the attractor under full map, A_{F_β}, is also transitive under F_β.

Proof: This proof will consist of two parts. First, we will show that circles passing through chunks of wedges eventually are wrapped around circles (as previously done twice). Second, we will show that in A_{F_β} there exists a circle close to any given circle that maps close to another given circle .

Preliminaries: Suppose β is chosen such that $K_{\mathcal{M}_\beta} = K(\mathcal{M}_\beta)$ is non-empty. Then Theorem 3.4 tells us $\mathcal{M}_\beta$ has an attractor, $A_{\mathcal{M}_\beta}$, and $\mathcal{M}_\beta|_{A_{\mathcal{M}_\beta}}$ is transitive. Since $K_{\mathcal{M}_\beta}$ is non-empty, $K(F_\beta) = K_{F_\beta}$ is also non-empty and A_{F_β} is the equivalent attractor under F_β. Consider any $x, y \in A_{F_\beta}$ with an arbitrary $\epsilon > 0$. For notational purposes, let the polar representation for x and y be $r_x e^{i\theta_x}$ and $r_y e^{i\theta_y}$ respectively. It follows that the circles of radii r_x and r_y (C_{r_x} and C_{r_y}) are also in K_{F_β}. Then, consider the open ϵ balls centered at x and y, denoted $B_\epsilon(x)$ and $B_\epsilon(y)$. We know there exist some $\delta_r(x) > 0$ and $0 < \delta_\theta(x) < \pi$ such that $W(x) \subset B_\epsilon(x)$. (See Figure 3.10.) The same is true for y: there exists some $\delta_r(y) > 0$ and $0 < \delta_\theta(y) < 2\pi$ such that $W(y) \subset B_\epsilon(y)$. However, we remark that the choice for $\delta_r(x)$ may not work for $\delta_r(y)$ and vice verse. Same is true for $\delta_\theta(x)$ and $\delta_\theta(y)$. But defining $\delta_\theta = \min\{\delta_\theta(x), \delta_\theta(y)\}$ and $\delta_r = \min\{\delta_r(x), \delta_r(y)\}$ will avoid this minor issue.

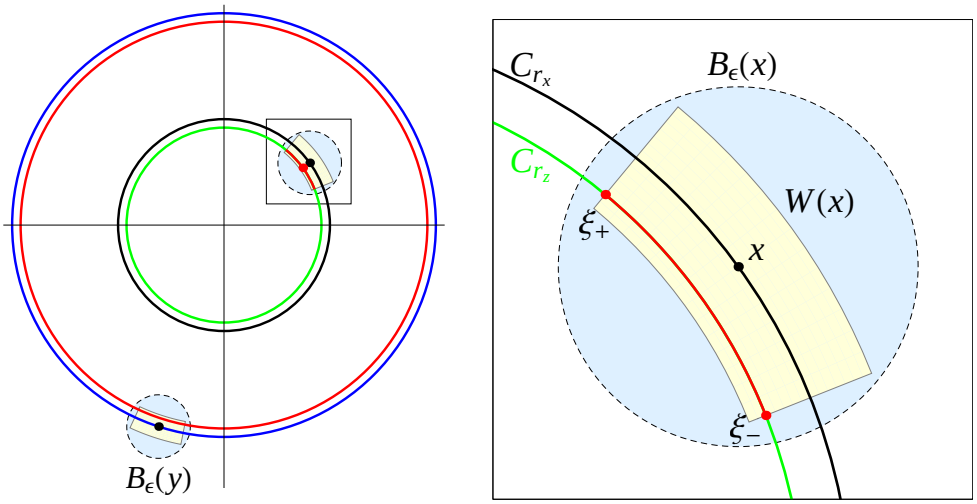

FIGURE 3.10: (*Left*) shows the circle of radius r_x (black), the circle of radius r_y (blue) and the circle of radius r_z (green). In addition $B_\epsilon(y)$ and $B_\epsilon(x)$ are visible. (*Right*) shows a zoom of $B_\epsilon(x)$ and some of the key players of the proof of Lemma 3.7. Note that the red interval, $C_{r_z} \cap W(x)$, is eventually wrapped around and displayed near C_{r_y} in Left.

PART 1: Let $x = r_x e^{i\theta_x}$ and consequently $C_{r_x} = \left\{r_x e^{i\theta} : 0 \leq \theta < 2\pi\right\}$ be given. Consider $W(x)$ defined by δ_θ and δ_r in the preliminaries and suppose some circle, $C_{r_z} = \left\{r_z e^{i\theta} : 0 \leq \theta < 2\pi\right\}$ passes through $W(x)$. Then $F_\beta^{(k)}(C_{r_z} \cap W(x))$ forms a geometric circle.

We can define C_{r_z} as follows.

$$C_{r_z} \cap W(x) = \left\{r_z e^{i\theta} : \theta_x - \delta_\theta \leq \theta \leq \theta_x + \delta_\theta\right\}.$$

This is illustrated in Figure 3.10 Right as the red curve contained in $W(x)$. Choose $k \in \mathbb{N}$ such that $k > \log_n(\pi/\delta_\theta)$. Since any $z \in C_{r_z}$ has the same magnitude (they lie on the same circle) and using the fact that circles centered at the origin map to circles centered at the origin, we know the magnitude of the k^{th} iterate for each z with have the same magnitude as well, $\mathcal{M}_\beta^{(k)}(r_z)$. Like Lemmas 3.3 and 3.5, consider the endpoints of the interval of angles for $C_{r_z} \cap W(x)$, defined to be $\xi_- = \theta_x - \delta_\theta$ and $\xi_+ = \theta_x + \delta_\theta$. From (12), $\left|\xi_+^{(k)} - \xi_-^{(k)}\right|$ is as follows.

$$\begin{aligned}\left|\xi_+^{(k)} - \xi_-^{(k)}\right| &= \left|\left[n^k(\theta_x + \delta_\theta) + \sum_{i=0}^{k-1} n^i \cdot \Omega_\beta(r_{k-1-i})\right]\right. \\ &= \left. -\left[n^k(\theta_x - \delta_\theta) + \sum_{i=0}^{k-1} n^i \cdot \Omega_\beta(r_{k-1-i})\right]\right| \\ &= \left|n^k\theta_x + \delta_\theta n^k - n^k\theta_x + \delta_\theta n^k\right| \\ &= 2\delta_\theta n^k\end{aligned}$$

Since k was chosen so that $k > \log_n(\pi/\delta_\theta)$, it follows that $\left|\xi_+^{(k)} - \xi_-^{(k)}\right| > 2\pi$ and

$$F_\beta^{(k)}(C_{r_z} \cap W(x)) = \left\{\mathcal{M}_\beta^{(k)}(r_z)\, e^{i\theta} : \xi_-^{(k)} \leq \theta < \xi_+^{(k)}\right\}.$$

However, under the context of F_β, where angles are taken modulo 2π, we get

$$F_\beta^{(k)}(C_{r_z} \cap W(x)) = \left\{\mathcal{M}_\beta^{(k)}(r_z)\, e^{i\theta} : 0 \leq \theta < 2\pi\right\}$$

and $F_\beta^{(k)}(C_{r_z} \cap W(x))$ forms a complete geometric circle.

Part 2: Now for the second part, suppose any two circles of radius r_x and r_y (C_{r_x} and C_{r_y}) are given in A_{F_β} and suppose some $\delta_r > 0$ and $0 < \delta_\theta < \pi$ are chosen (as in Part 1). The two circles correspond to r_x and r_y in $\mathbb{R}^+$ under $\mathcal{M}_\beta$ by the properties developed earlier in the paper. Next consider the one-dimensional open neighborhood of radius δ_r about r_x and r_y, denoted $N_{\delta_r}(r_x)$ and $N_{\delta_r}(r_y)$. Since $\mathcal{M}_\beta$ is transitive and both $N_{\delta_r}(r_x)$ and $N_{\delta_r}(r_y)$ are non-empty open sets, their hitting times are infinite (Theorem 3.6).

$$\mathcal{H}_{r_x,r_y} = \mathcal{H}(N_{\delta_r}(r_x), N_{\delta_r}(r_y)) = \{k_1, k_2, k_3, \cdots\}$$

Since $\mathcal{H}_{r_x,r_y}$ is an infinite subset of $\mathbb{N}$, there must exist some $k \in \mathcal{H}_{r_x,r_y}$ (really an infinity of k's) such that $k > \log_n(\pi/\delta_\theta)$. Then, k corresponds to some $r_z \in N_{\delta_r}(r_x)$ such that $\mathcal{M}_\beta^{(k)}(r_z) \in N_{\delta_r}(r_y)$. Finally under the full map, F_β, the analogous reasoning says the same k implies C_{r_z} starts within δ_r of C_{r_x} (in magnitude) and after k iterates is within δ_r of C_{r_y} (in magnitude).

Putting Part 1 and Part 2 together, let $x = r_x e^{i\theta_x}, y = r_y e^{i\theta_y} \in \mathbb{C}$ be given along with some $\epsilon > 0$. There exists some $\delta_r > 0$ and $0 < \delta_\theta < \pi$ such that $W(x) \subset B_\epsilon(x)$ and

$W(y) \subset B_\epsilon(y)$. Then, Part 2 results in $W(x) \cap C_{r_z} \neq \emptyset$ for some C_{r_z} and $k > \log_n(\pi/\delta_\theta)$. Furthermore, $W(x) \cap C_{r_z}$ is the red curve in Figure 3.10 Right and $F_\beta^{(k)}(W(x) \cap C_{r_z})$ is within δ_r of C_{r_y} (in magnitude). Since $k > \log_n(\pi/\delta_\theta)$, $F_\beta^{(k)}(W(x) \cap C_{r_z})$ forms a complete geometric circle and it follows that $F_\beta^{(k)}(W(x) \cap C_{r_z}) \cap W(y)$ is non-empty. With that observation, there exists some $z \in W(x) \cap C_{r_z} \subset B_\epsilon(x)$ such that $F_\beta^{(k)}(z) \in F_\beta^{(k)}(C_r \cap W(x)) \cap W(y) \subset B_\epsilon(y)$. The point z starts withing ϵ of x and iterates within ϵ of y. Therefore if $\mathcal{M}_\beta|_{A_{\mathcal{M}_\beta}}$ is transitive, then $F_\beta|_{A_{F_\beta}}$ is transitive. ■

Now suppose periodic points are dense in the attractor under $\mathcal{M}_\beta$. We can state a similar result to Lemma 3.7 as follows.

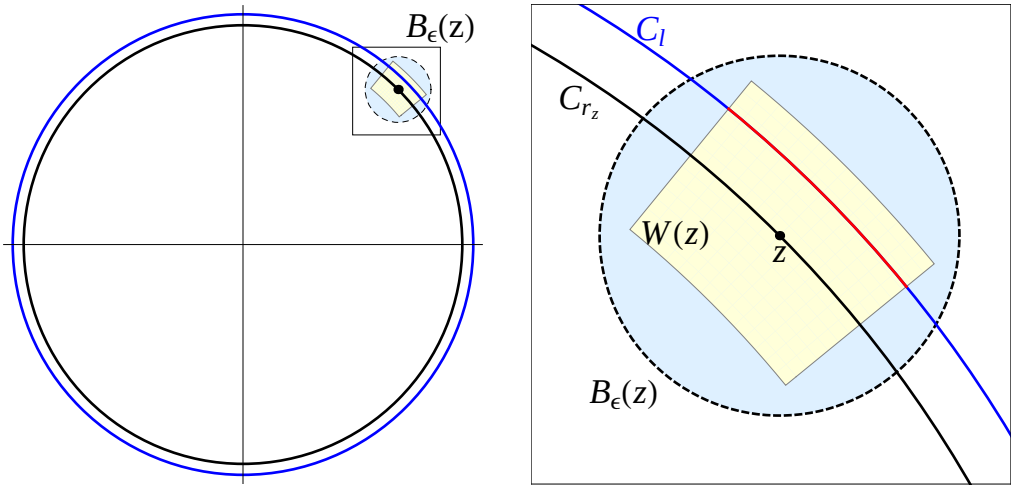

FIGURE 3.11: (*Left*) shows a circle of radius r_z and an $\epsilon-$neighborhood of the point z on that circle. Since periodic points are dense under $\mathcal{M}_\beta$, there must be a circle (blue) that passes through $W(z)$. (Right) shows a zoomed in portion of Left along with the red set, $C_l \cap W(z)$ that is guaranteed to exist by the argument in Lemma 3.8.

LEMMA 3.8 *Dense Periodic Points under $\mathcal{M}_\beta$ Implies Dense Periodic Points under F_β* - Suppose β is chosen so that periodic points are dense in the attractor, $A_{\mathcal{M}_\beta}$, under $\mathcal{M}_\beta$. Then, periodic points are dense in the equivalent attractor, A_{F_β}, under F_β.

Proof: Suppose $K(\mathcal{M}_\beta)$ and $K(F_\beta)$ are non-empty. Then the attractors $A_{\mathcal{M}_\beta}$ and A_{F_β} exist and by assumption periodic points are dense in $A_{\mathcal{M}_\beta}$ under $\mathcal{M}_\beta$. Let $z = r_z e^{i\theta_z} \in A_{F_\beta}$ and it must be true that $r_z \in A_{\mathcal{M}_\beta}$. Also, let an arbitrary $\epsilon > 0$ be given and consider the open ϵ ball about z, $B_\epsilon(z)$. As with the previous arguments, there exists an $\delta_r(z) > 0$ and $0 < \delta_\theta(z) < \pi$ such that $W(z) \subset B_\epsilon(z)$. Since periodic points are dense under $\mathcal{M}_\beta$, there must exist some period l circle, C_l, within δ_r (in magnitude) of C_{r_z} and thus $C_l \cap W(z)$ is nonempty. Choosing $l \cdot k > \log_n(\pi/\delta_\theta)$ implies that $F_\beta^{(l\cdot k)}(C_l \cap W(z)) = C_l$, similar to Lemma 3.5. The red interval in Figure 3.11 Right is wrapped around C_l and there must exists some $p = r_p e^{i\theta_p} \in C_l \cap W(z)$ such that $\mathcal{M}_\beta^{(l)}(r_p) = r_p$ and $\mathcal{A}_\beta^{(k)}(r_p, \theta_p) = \theta_p$. Therefore p is a period $\operatorname{lcm}\{l, k\}$ point within ϵ of z, an arbitrary point in A_{F_β}. ■

Corollary 3.9: *Chaos under $\mathcal{M}_\beta$ implies Chaos under F_β* - Suppose an attractor under $\mathcal{M}_\beta$ exists and is chaotic. Then the equivalent attractor under F_β is chaotic.

Proof: See Lemmas 3.7 and 3.8. ■

Theorem 3.10: Let there exist an attractor, $A_{\mathcal{M}_\beta}$, under $\mathcal{M}_\beta$ and let A_{F_β} be the analogous attractor under F_β.

1. If $A_{\mathcal{M}_\beta}$ is periodic, then A_{F_β} is chaotic.
2. If $A_{\mathcal{M}_\beta}$ is a minimal Cantor set, then A_{F_β} is transitive, but not chaotic.
3. If $A_{\mathcal{M}_\beta}$ is the orbit of a periodic interval, then $A_{F_\beta}$is chaotic.

Proof:

(1): If $A_{\mathcal{M}_\beta}$is a periodic point, then A_{F_β} consists of periodic circles. In any case Lemma 3.5 proves A_{F_β} is chaotic.

(2): If A_{F_β} is a minimal Cantor set of Circles, then $A_{\mathcal{M}_\beta}$ is a minimal Cantor set of points. Here, $\mathcal{M}_\beta|_{A_{\mathcal{M}_\beta}}$ is transitive by Theorem 3.4. So $F_\beta|_{A_{F_\beta}}$ is transitive as well (Lemma 3.7). However, since $A_{\mathcal{M}_\beta}$ is a minimal Cantor set of points, there exists no

invariant subsets of $A_{\mathcal{M}_\beta}$. Since periodic orbits are invariant subsets, $A_{\mathcal{M}_\beta}$ does not have any periodic orbits and it follows that A_{F_β} is not chaotic.

(3): If A_{F_β} is the orbit of a periodic interval, then A_{F_β} is transitive (Theorem 3.4). Therefore $F_\beta|_{A_{F_\beta}}$ is transitive as well (Lemma 3.7). Also, since $A_{\mathcal{M}_\beta}$ is the orbit of a periodic interval, it is clear that periodic points are dense. Thus periodic points are dense for A_{F_β} under F_β. Therefore, $F_\beta|_{A_{F_\beta}}$ is chaotic. ■

We should remark that every attractor for F_β must be transitive because of Theorem 3.10. It also follows that most of the attractors behave chaotically, with the exception to the minimal Cantor set case. However, there are few β values that yield a minimal Cantor sets. Thus most of the attractors are chaotic attractors.

The final case is as follows and covers all β values to the left of the black band in the β parameter plane.

Theorem 3.11: If $K(\mathcal{M}_\beta)$ is a Cantor set, then $K(F_\beta)$ is a chaotic Cantor set of geometric circles.

Proof: If $K(\mathcal{M}_\beta)$ is a Cantor set, then $K(\mathcal{M}_\beta)$ is both transitive and has dense periodic orbits under $\mathcal{M}_\beta$. Therefore $K(\mathcal{M}_\beta)$ is chaotic and Theorem 3.2.3 and Corollary 3.9 provide insight as to why $K(F_\beta)$ is a Cantor set of geometric circles whose dynamics are chaotic under F_β. ■

In the previous sub-section we were able to breakdown all possible fates of orbits by classifying them into three distinct types of sets, two of which have sets of points whose orbits remain bounded under iteration of F_β (The Modulus Trichotomy). Then, in this sub-section Theorems 3.10 and 3.11 give further insight into the dynamics within those sets and we can update the Modulus Trichotomy stated in Theorem 3.2.

An Updated Dynamical Trichotomy - Given the map F_β defined in (3), then the dynamics fall into one of three categories.

1. If the critical orbit tends to infinity strictly monotonically, then the set of points which remain bounded is an empty set. All points are attracted to ∞. This corresponds to the area to the right of the black band in the β parameter plane (Theorem 3.2.1).

2. If the critical orbit remains bounded, then the set of points that remain bounded has an attractor A_{F_β}, and in every case this attractor is transitive. In most cases this attractor is chaotic. This corresponds to parameter values chosen in the black band in the β parameter plane.

3. If the critical orbit tends to infinity, but non monotonically, then the set of points that remain bounded is a Cantor set of geometric circles whose dynamics are chaotic (Theorem 3.11). This corresponds to parameter values chosen to the left of the black band in the β parameter plane.

At the beginning of this section, we set out to understand the complete dynamics for the simplest case, F_β, of these non-analytic singular perturbations and the previous summary does just that. However, we will address some further properties of the bounded orbits in the next sub-section.

3.6 Bifurcation Curves and Why $n = 2$ is Different.

In the previous sub-section, we were able to summarize all possible dynamics. However, in this sub-section we want to provide some further insight into the structure of the black band in the β parameter plane, and more specifically, illustrate the bifurcation curves. Earlier we had mentioned the unbounded curve contained in the black band that yields fixed critical orbits. Furthermore, we were able to find an explicit equation for this curve in (11). Through numerical continuation algorithms we can find other curves in the black band that yield other superattracting periodic critical orbits. You can find the *Mathematica* code using Newton's Method to find and plot these curves in the appendix of this paper. Figure 3.12 shows a few of these bifurcation curves in the β

parameter plane. Figure 3.12 Left and Middle display the same windows as Figure 3.4 for $n = 3$, with an additional zoom in Figure 3.12 Right. Any β value chosen on the the green curve yields a superattracting fixed critical orbit. The red, orange, and blue curves yield superattracting periods 2, 4, and 3 respectively. The black curve is the left boundary of the black band where the critical orbit is fixed after two iterates.

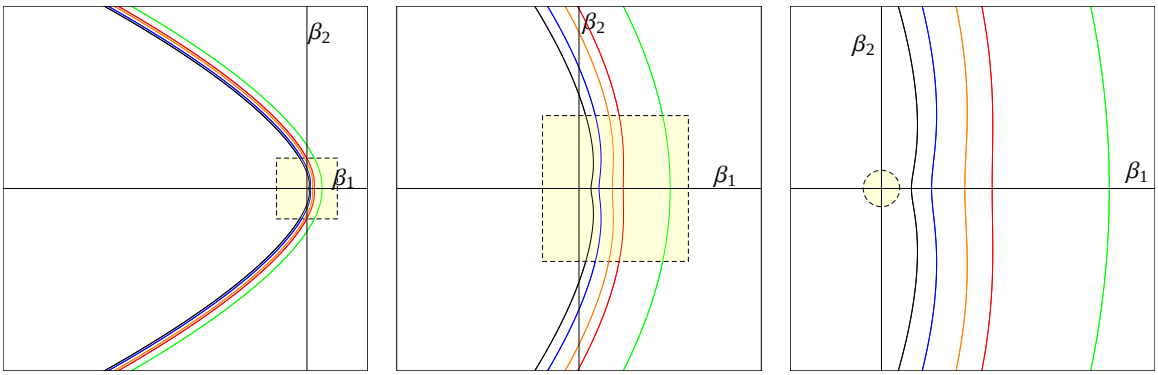

FIGURE 3.12: The β parameter plane for $n = 3$. (*Left*) displays a window of $[-2.5, 0.5] \times [-1.5, 1.5]\, i$ with successive zooms (*Middle*) and (*Right*). Right also shows the open set about the origin that does not intersect the prefixed curve.
The colors represent a critical orbit that is a
Green - Superattracting Fixed Point,
Red - Superattracting Period 2 Orbit,
Orange - Superattracting Period 4 Orbit,
Blue - Superattracting Period 3 Orbit, and
Black - Prefixed after two iterates.

It is interesting to point out that all of these curves are smooth, but for the superattracting periodic curves greater than 1 appear to bend backwards. At first, it was unclear that these curves were indeed smooth, but numerical experiments suggest that this is the case. Furthermore, if you fix $\phi \neq \pi$ for $\beta = |\beta|\, e^{i\phi}$ and vary $|\beta|$ as in Figure 3.4 you will find that as $|\beta| \to 0$, the function F_β goes through the period doubling route to chaos as it crosses these bifurcation curves. Also, these curves all appear similar for $n \geq 3$ and [Pe3] shows that as $n \to \infty$, every one of these curves approaches a single limiting parabola . Also, Figure 3.12 Right illustrates the fact that there exists an open set about the origin that does not intersect the left boundary of the black band (black curve). We will see that this is not the case for $n = 2$.

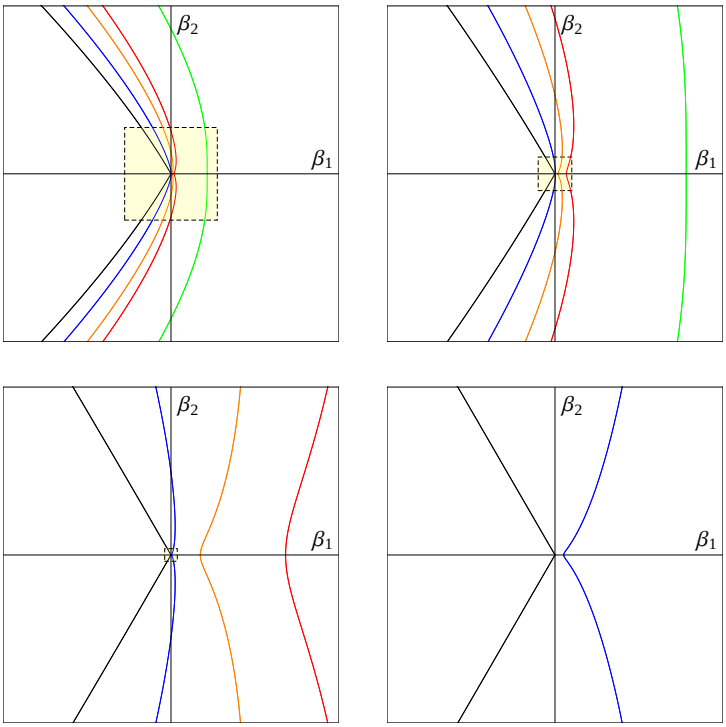

FIGURE 3.13: the β parameter plane for $n = 2$ and successive zooms. Note that every open set about the origin intersects the (black) prefixed curve, a difference from the $n > 2$ cases.
The colors represent a critical orbit that is a
Green - Superattracting Fixed Point,
Red - Superattracting Period 2 Orbit,
Orange - Superattracting Period 4 Orbit,
Blue - Superattracting Period 3 Orbit, and
Black - Prefixed after two iterates.

Figure 3.13 shows the same bifurcation curves for $n = 2$, but it is easy to see that things are slightly different. First, we notice that the prefixed and period 2, 3, and 4 curves are very close to the origin. This differs from the cases $n \geq 3$. We can explicitly calculate why this is the case. Fix the angle, ϕ, of the β value such that $-\pi < \phi < \pi$. Then consider the second iterate of the critical point as calculated in (10).

$$\mathcal{M}_\beta^{(2)}\left(|\beta|^{1/2n}\right) = \sqrt{2^n |\beta|^n (1+\cos\phi)^n + 2|\beta|\cos\phi + \frac{|\beta|^2}{2^n |\beta|^n (1+\cos\phi)^n}}$$

Limiting towards the origin yields the following.

$$\lim_{|\beta|\to 0} \mathcal{M}_\beta^{(2)}\left(\left|\beta^{1/2n}\right|\right) = \begin{cases} \infty & n > 2 \\ \frac{1}{2(1+\cos\phi)} & n = 2 \end{cases}$$

The above calculation shows that for $n > 2$ we can make the second iterate arbitrarily large as the magnitude of the β value decreases. This is not the case for $n = 2$ and it is precisely this reason why we cannot draw an open set about the origin for the case $n = 2$. The above calculation also tells us that the black/prefixed curve is not smooth as it passes over the horizontal axis. The second iterate never passes through the trap door, T, for certain small β values. For Devaney's family, [De3] gets a similar result distinguishing the cases $n > 2$ from $n = 2$.

One last result deals with these bifurcation curves. Initially it was proposed that since the prefixed (black) curve is not smooth for $n = 2$, there may be other bifurcation curves for different periods that are also non-smooth. [Pe3] proved that given any period k curve that passes close to the origin, that there must exist a period $k + 1$ curve that passes between the origin and the period k curve, providing the evidence that every superattracting periodic curve is smooth and crosses the positive β_1 axis.

That concludes our study of the simplest case of the family defined in (1). We had some nice properties that allowed us to simplify the arguments and we were able to prove some nice results. This will provide valuable insight into other cases of (1) as well. However, all other cases do not result in a decoupled modulus map, which makes the study more difficult. The next section describes various paths that this study is heading down in the future as well as proposing some nice open questions and conjectures.

4 Further Study

Due to the time restrictions of the study, the simplest case ($n = d$ and $c = 0$) was the only family we could describe with certainty. However, we have done many experiments to help understand and hypothesize about the other cases. This section points the reader into the direction of where this study is heading in future.

4.1 $(z, \bar{z})$ Coordinates

Like [Pe1] and [Pe2], another way to define the full map would be using $(z, \bar{z})$ coordinates. Recall the (slightly modified) definition in (1).

$$F_{\beta,c}(z, \bar{z}) = z^n + c + \frac{\beta}{\bar{z}^d}$$

Without justifying the details, we can define $R_{\beta,c}$ as follows.

$$R_{\beta,c}\begin{pmatrix} z \\ \bar{z} \end{pmatrix} = \begin{pmatrix} f_{\beta,c}(z, \bar{z}) \\ g_{\beta,c}(z, \bar{z}) \end{pmatrix} = \begin{pmatrix} F_{\beta,c}(z, \bar{z}) \\ \overline{F_{\beta,c}(z, \bar{z})} \end{pmatrix} = \begin{pmatrix} z^n + c + \frac{\beta}{\bar{z}^d} \\ \bar{z}^n + \bar{c} + \frac{\bar{\beta}}{z^d} \end{pmatrix}$$

[N1] and [N2] study the importance of critical curves, J_0, and their orbits under iteration. In our context, J_0 would be solutions to $\left|J_{R_{\beta,c}}\right| = 0$ where $J_{R_{\beta,c}}$ is the Jacobian matrix of $R_{\beta,c}$.

$$\begin{aligned}
\left|J_{R_{\beta,c}}\right| &= \begin{vmatrix} \frac{\partial f_{\beta,c}}{\partial z} & \frac{\partial f_{\beta,c}}{\partial \bar{z}} \\ \frac{\partial g_{\beta,c}}{\partial z} & \frac{\partial g_{\beta,c}}{\partial \bar{z}} \end{vmatrix} \\
&= \begin{vmatrix} nz^{n-1} & -\frac{d\beta}{\bar{z}^{d+1}} \\ -\frac{d\bar{\beta}}{z^{d+1}} & n\bar{z}^{n-1} \end{vmatrix} \\
&= \left(nz^{n-1}\right)\left(n\bar{z}^{n-1}\right) - \left(\frac{d\beta}{\bar{z}^{d+1}}\right)\left(\frac{d\bar{\beta}}{z^{d+1}}\right) \\
&= n^2 |z|^{2(n-1)} - \frac{d^2 |\beta|^2}{|z|^{2(d+1)}}
\end{aligned}$$

Now we can solve $\left|J_{R_{\beta,c}}\right| = 0$.

$$\begin{aligned}
n^2 |z|^{2(n-1)} - \frac{d^2 |\beta|^2}{|z|^{2(d+1)}} &= 0 \\
n^2 |z|^{2(n-1)} &= \frac{d^2 |\beta|^2}{|z|^{2(d+1)}} \\
\sqrt{n^2 |z|^{2(n-1)}} &= \sqrt{\frac{d^2 |\beta|^2}{|z|^{2(d+1)}}} \\
n |z|^{n-1} &= \frac{d |\beta|}{|z|^{d+1}} \\
|z|^{n+d} &= \frac{d}{n} |\beta| \\
|z| &= \left(\frac{d}{n} |\beta|\right)^{\frac{1}{n+d}} \qquad (14)
\end{aligned}$$

Here, the critical curve is still a circle but for a much more general family of maps. Now recall when $n = d$, the critical circle was $|z| = |\beta|^{1/2n}$, which agrees with $n = d$ in (14). However, we derived them in two different contexts. Either way, the critical set J_0, is a geometric circle about the origin and we hypothesis that the dynamics for (1) depend somehow on J_0.

4.2 Parameter Plane Arrays

No knowledge of critical sets is needed to create dynamic plane images. So before any of the theory of this project was derived, we were creating bounded/unbounded dynamic plane images. To visualize what a parameter plane may look like, we made an array of dynamic planes to form the parameter plane array. The parameter plane array displayed in Figure 4.1 gives clues to the structure of the parameter plane. By observing the individual dynamic spaces contained in the parameter plane array in Figure 4.1 Left, we were able to guess that there exists only three dynamics planes possible (The Modulus Trichotomy) and that they occured in some parabola like band in the parameter plane. It's an interesting method for making conjectures and for that case, it turned out to be correct.

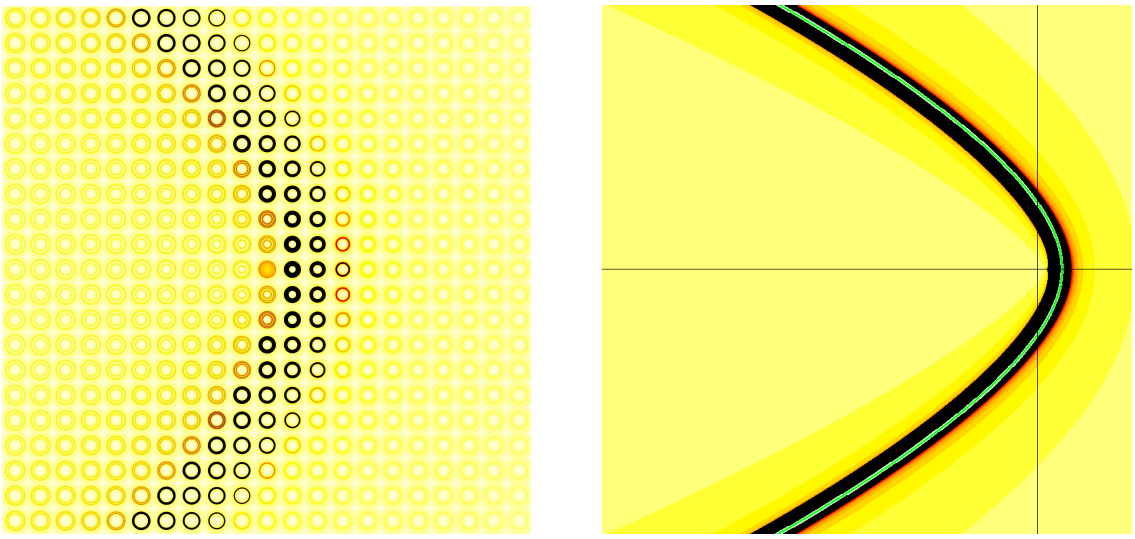

FIGURE 4.1: A parameter plane array (Left) gives us an idea of what the actual parameter plane (Right) is for $z^3 + \beta/\bar{z}^3$.

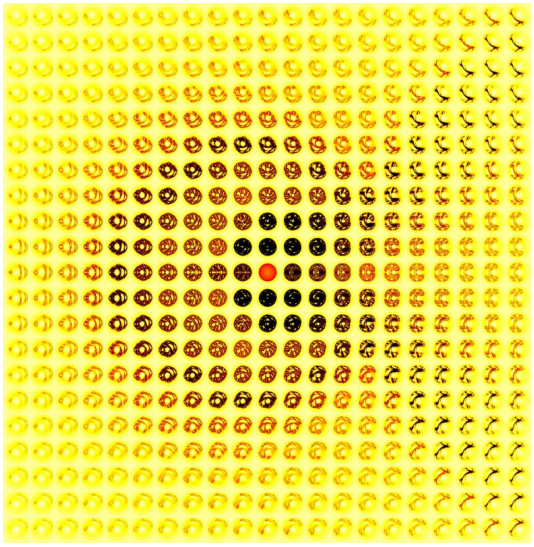

FIGURE 4.2: A parameter plane array for $z^2 + \beta/\bar{z}$. A guess for its actual parameter plane is displayed in Figure 4.3.

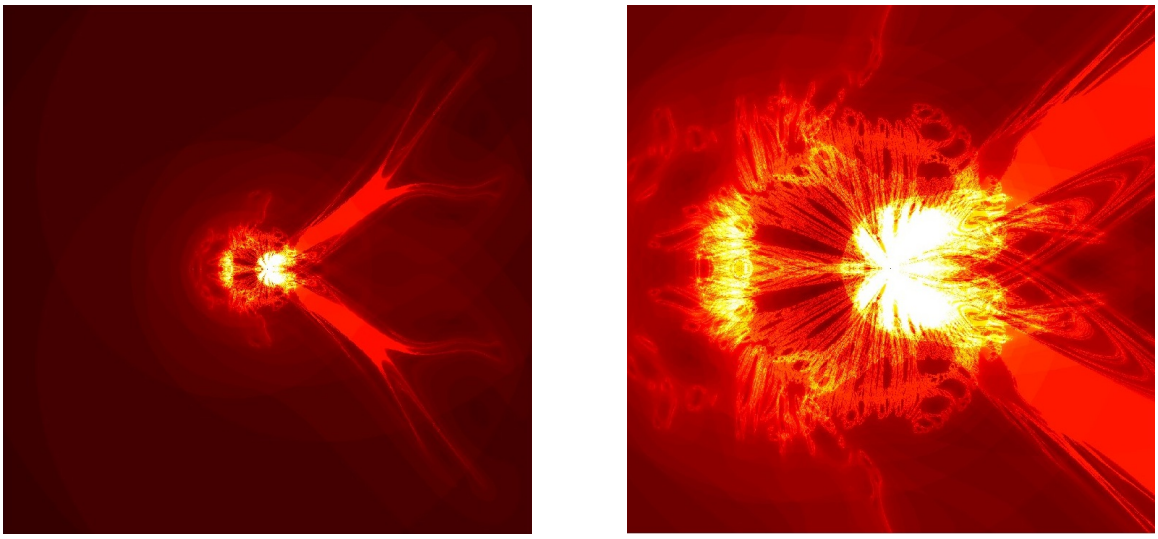

FIGURE 4.3: A guess for the parameter plane for $z^2 + \beta/\bar{z}$ (Left) and a zoom (Right). These images tracked three critical points on the critical circle defined above. If all three critical points remain bounded under iteration, then the point is colored white. In general the darker the color, the quicker the critical point(s) escapes. The lighter non-white regions suggest that some critical points remain bounded while others do not.

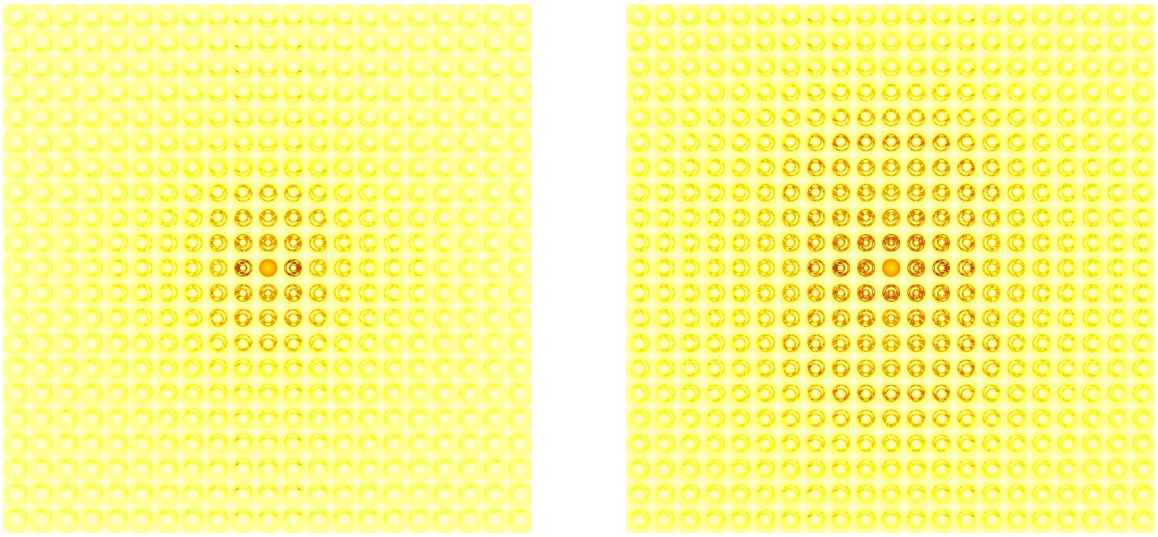

FIGURE 4.4: A parameter plane array for $z^3 + \beta/\bar{z}^2$ (*Left*) and a zoom (*Right*). A guess as to the actual parameter plane is displayed in Figure 4.5.

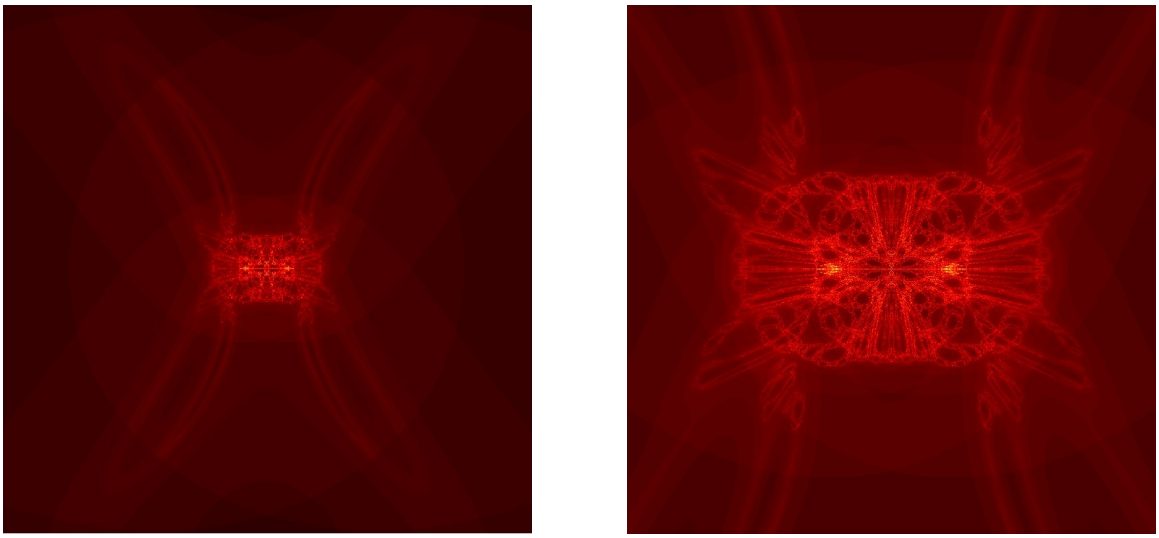

Figure 4.5: A guess for the parameter plane for $z^3 + \beta/\bar{z}^2$ (*Left*) and a zoom (*Right*) with the color scheme described in Figure 4.3.

Let us explain the images above. The parameter plane arrays give actual dynamic planes laid out in such a way that the structure of the parameter plane might be visible. The images with guesses of the parameter planes are a little more involved. First, it is clear that the critical circle derived earlier is very important in the structure of the parameter plane as well as the individual dynamic planes. However, it is difficult to iterate an entire circle because an infinity of points lie on it. So Figures 4.3 and 4.5 choose only three values on the critical circle and iterate them under F_β. If all three points remain bounded under iteration, we color the point white. In this case, this suggests that the entire circle remains bounded. The white or lighter colors indicate that some points on the critical circle remain bounded. Another tricky aspect here is that the critical circle does not have to behave in a symmetric fashion. That is, it is possible that some parts of the critical circle remain bounded while others do not. So the images created in Figures 4.3 and 4.5 are a crude guess to the actual parameter plane. In the future, we would like to improve this algorithm as we explore more of the theory to either verify or improve our guesses. However, we have enough information to make a conjecture to verify in the future.

Conjecture: Given $F_\beta(z) = z^n + \beta/\bar{z}^{n-1}$ for $n \geq 3$, the bounded sets under F_β can never have

positive measure.

To illustrate the conjecture, see Figures 4.4 and 4.5. In Figure 4.4, there are no dynamic planes that seem to have bounded sets with positive measure. No black sets. Furthermore, in Figure 4.5 it appears that the set of white points has zero measure. This observation has been confirmed for $n = 3$ with $d = 2$, $n = 4$ with $d = 3$, and $n = 5$ with $d = 4$. As a contrast, see Figures 4.2 and 4.3. Here it is clear that there exists some dynamic spaces in Figure 4.2 that have sets of bounded orbits with positive measure. Then in Figure 4.3, we see many white points. Enough it appears, to create a set with positive measure in a butterfly like arrangement. Another observation is that the planes with black sets in Figure 4.2 correspond to white points in Figure 4.3, as one might expect. The final remark is that these experimental plane images appear nothing like that of the simple case $n = d$ studied for the majority of this paper. So there is much more to study, not only in this field, but in this specific family of maps.

5 Algorithms & Codes

5.1 Parameter Plane

Below is code, written in QtOctave, for creating images of parameter planes. All of the parameter plane images use code similar to below.

```
%%%%%%%%%%%%%%%%%%%%%%%%%%%%%%%%%%%%%%%%%%%%%%%%%%%%%%%%%%%%%%%%%%%%%%%
%%%%%%%%%%%%%%%%%    Parameter Plane     %%%%%%%%%%%%%%%%%%%
%%%%%%%%%%%%%%%%%%%%%%%%%%%%%%%%%%%%%%%%%%%%%%%%%%%%%%%%%%%%%%%%%%%%%%%

n=2;            %% power of F0 and pole
imin=-1.5;      %% imaginary part minimum
imax=1.5;       %% imaginary part maximum
rmin=-1.5;      %% real part minimum
rmax=1.5;       %% real part maximum
step=.001;      %% step size/ distance between nodes
itmax=20;       %% maximum number of iterates allowed

%%%%%%%%%%%%%%%%%%%%%%%%%%%%%%%%%%%%%%%%%%%%%%%%%%%%%%%%%%%%%%%%%%%%%%%

rnum=floor((rmax-rmin)/step+1);  %%  number of imag. nodes
inum=floor((imax-imin)/step+1);  %%  number of real nodes
A=zeros(rnum,inum);    %%  empty array: parameter values
B=zeros(rnum,inum);    %%  empty array: function values
ITER=zeros(rnum,inum); %%  empty array: num. of iterations

function f=f(w,l1,l2,n)  %%  function of magnitudes squared
   f=w^n+2*l1+(l1^2+l2^2)/(w^n);
endfunction

%%%%%%%%%%%%%%%%%%%%%%%%%%%%%%%%%%%%%%%%%%%%%%%%%%%%%%%%%%%%%%%%%%%%%%%
%%%%%%%%%%%%%%%%%    Iteration Scheme   %%%%%%%%%%%%%%%%%%%
%%%%%%%%%%%%%%%%%%%%%%%%%%%%%%%%%%%%%%%%%%%%%%%%%%%%%%%%%%%%%%%%%%%%%%%

for j=1:rnum
   for k=1:inum
      A(j,k)=(rmin+step*(k-1))+(imax-(j-1)*step)*I;
      B(j,k)=2*sqrt(real(A(j,k))^2+imag(A(j,k))^2)+
2*real(A(j,k));                      %% critical value
      its=1;                         %% after 1 iterate
      while (norm(B(j,k))<10&&its<itmax)
         B(j,k)=f(B(j,k),real(A(j,k)),imag(A(j,k)),n);
         its++;
      endwhile
      ITER(j,k)=its;
   endfor
   percent=j/rnum*100    %% updates status of iteration
endfor
```

```
%%%%%%%%%%%%%%%%%%%%%%%%%%%%%%%%%%%%%%%%%%%%%%%%%%%%%%%%%%%%%%%%%%%%%%%
%%%%%%%%%%%%%%%%%%%%%%%%%%%%%%%%%%%%%%%%%%%%%%%%%%%%%%%%%%%%%%%%%%%%%%%
%%%%%%%%%%%%%%%%%%%%%%%%%%%%%%%%%%%%%%%%%%%%%%%%%%%%%%%%%%%%%%%%%%%%%%%

colormap(hot(itmax));
image(-(ITER-itmax))
axis('square','nolabel','off')
```

5.2 Dynamic Plane

Below is code, written in QtOctave, for creating images of dynamic planes. All images of dynamic planes have code similar to this.

```
%%%%%%%%%%%%%%%%%%%%%%%%%%%%%%%%%%%%%%%%%%%%%%%%%%%%%%%%%%%%%%%%%%%%%%%
%%%%%%%%%%%%%%%%%%%%%%%%%%%%%%%%%%%%%%%%%%%%%%%%%%%%%%%%%%%%%%%%%%%%%%%
%%%%%%%%%%%%%%%%%%%%%%%%%%%%%%%%%%%%%%%%%%%%%%%%%%%%%%%%%%%%%%%%%%%%%%%

%%%%%%%%%%%%%%%%%%%%%%%%%%%%%%%%%%%%%%%%%%%%%%%%%%%%%%%%%%%%%%%%%%%%%%%
%%%%%%%%%%%%%%%%%%%%%%%%%%%%%%%%%%%%%%%%%%%%%%%%%%%%%%%%%%%%%%%%%%%%%%%
%%%%%%%%%%%%%%%%%%%%%%%%%%%%%%%%%%%%%%%%%%%%%%%%%%%%%%%%%%%%%%%%%%%%%%%

n=2;       %% Power of the function
imin=-1.5; %% imaginary minimum
imax=1.5;  %% imaginary maximum
rmin=-1.5; %% real minimum
rmax=1.5;  %% real maximum
step=0.01; %% step size/ distance to the next node
itmax=25;  %% maximum number of iterates allowed

%%%%%%%%%%%%%%%%%%%%%%%%%%%%%%%%%%%%%%%%%%%%%%%%%%%%%%%%%%%%%%%%%%%%%%%

rnum=floor((rmax-rmin)/step+1); %% num. of imag. nodes
inum=floor((imax-imin)/step+1); %% num of real nodes
A=zeros(rnum,inum);             %% array of func. values
ITER=zeros(rnum,inum);          %% array of # of iterations
function f=f(z,c,n)
   f=(z^n)+c/(conj(z)^(n));
endfunction

%%%%%%%%%%%%%%%%%%%%%%%%%%%%%%%%%%%%%%%%%%%%%%%%%%%%%%%%%%%%%%%%%%%%%%%
%%%%%%%%%%%%%%%%%%%%%%%%%%%%%%%%%%%%%%%%%%%%%%%%%%%%%%%%%%%%%%%%%%%%%%%
%%%%%%%%%%%%%%%%%%%%%%%%%%%%%%%%%%%%%%%%%%%%%%%%%%%%%%%%%%%%%%%%%%%%%%%

lambda=whatever_you_want;
for j=1:rnum
   for k=1:inum
   A(j,k)=(rmin+step*(k-1))+(imax-(j-1)*step)*I;
   its=0;
```

```
   while (norm(A(j,k))<10&&its<itmax)
      A(j,k)=f(A(j,k),lambda,n);
      its++;
   endwhile
   endfor
endfor

h=figure(1);
colormap(hot(itmax));
image(-1(ITER-itmax));
title(['\z^',num2str(n),'+',num2str(lambda),'/conj(z)^'
   ,num2str(n)])
axis('square','nolabel','off');
print(h,'-djpeg',['plot',num2str(ind),'.jpeg'])
```

5.3 Bifurcation Curves

Below is an abbreviated code, written in *Mathematica*, for the continuation method for calculating bifurcation curves. It gives the basic algorithm. Then the bifurcation curves appear in two halves. Here plotper1 and plotper2 are these halves. Then simply call the ListPlot command in *Mathematica*.

```
M[r_,B_,P_,n_]:=Sqrt[r^(2n)+2B*Cos[P]+B^2/r^(2n)]
Mk[k_,r_,B_,P_,n_]:=Nest[M[#,B,P,n]&,r,k]
n=3; %%Specify map power
step=.001;
endangle=5Pi/6;
num=Floor[endangle/step]+1;
start1=0.125;   %%make start guesses from graphs
start2=0.06125;
start3=0.0275;
start4=0.0458;
starth=0.0165;
k1=1;  %%Enter whatever period here
per1=Table["",{i,1,num}];
Off[FindRoot::lstol]
For[
i=2,
i<num,
i++,
per1[[1]]=B/.FindRoot[Mk[k1,B^(1/(2n)),B,0,n]-B^(1/(2 n)),{B,start1}];
per1[[i]]=B/.FindRoot[Mk[k1,B^(1/(2n)),B,(i-1)*step,n]-B^(1/(2n)),
{B,per1[[i-1]]}];
]
plotper11=Table[{Re[per1[[i]]E^((i-1)*step*I)],Im[per1[[i]]E^((i-1)*step*I)]},
{i,1,num-1}];
plotper12=Table[{Re[per1[[i]]E^(-(i-1)*step*I)],Im[per1[[i]]E^(-(i-1)*step*I)]},
{i,1,num-1}];
```

References

[Ba] Banks, J., Brooks, J. Cairns G., Davis, G., and Stacey, P. On Devaney's Definition of Chaos. *The American Mathematical Monthly* Vol. 99, No. 4 (Apr. 1992), pp 332-334

[Bl1] Blanchard, P. and Chiu, A. Complex Dynamics: An Informal Discussion, *Fractal Geometry and Analysis*, (1991), pp 45-98

[Bl2] Blanchard, P. Complex Analytic Dynamics on the Riemann Sphere, *Bulletin of the American Mathematical Society*, Vol. 11, No. 1, (1984)

[De1] Devaney, R. A First Course in Chaotic Dynamical Systems, *Westview Press Perseus Books Publishing*, (1992)

[De2] Devaney, R. Singular Perturbations of Complex Analytic Dynamical Systems. *Nonlinear Dynamics and Chaos: Advances and Perspectives*, (2010), pp. 13-29

[De3] Devaney, R. Dynamics of $z^n+\lambda/z^n$; Why the Case $n = 2$ is Crazy. *Conformal Dynamics and Hyperbolic Geometry,* AMS Contemporary Mathematics, Vol. 573 (2012), pp. 49-65

[De4] Devaney, R., Look, D., and Uminsky, D. The Escape Trichotomy for Singularly Perturbed Rational Maps. *Indiana University Mathematics Journal*, Vol. 54, (2005), pp. 1621-1634

[De5] Devaney, R. and Russell, Elizabeth D. Connectivity of Julia Sets for Singularly Perturbed Rational Maps. Preprint (2012)

[deM vSt] de melo, W., van Strien, S. One-dimensional dynamics, Ergebnisse der Mathematik und ihrer Grenzgebiete, *Springer-Verlag*, Berlin, (1993)

[Dr] Drexler, J. A nonanalytic perturbation of complex quadratic family of maps, Master's Project University of Minnesota Duluth, Technical Report, (1996)

[Ko] Kolyada, S. and Snoha L. Topological Transitivity, *Scholarpedia* 4(2):5802, (2009)

[Kr1] Kraft, R. Chaos, Cantor Sets, and Hyperbolicity for the Logistic Maps, *The American Mathematical Monthly*, Vol. 106, No. 5 (1999), pp. 400-408

[Kr2] Kraft, R. Some One-Dimensional Dynamics, Preprint (2012)

[Mc1] McMullen, C., Automorphisms of Rational Maps, Holomorphic Functions and Moduli. Vol. 1, Math. Sci. Res. Inst. Publ. 100. *Springer*, New York, (1988)

[N1] Nien, C. The dynamics of Planar Quadratic Maps with Nonempty Bounded Critical Set. *International Journal of Bifurcation and Chaos*, Vol. 8, No. 1, (1998), pp. 95-105

[N2] Nien, C. The Investigation of Saddle Node Bifurcations With a Zero Eigenvalue - Includes Example of Non-Analyticity, Doctoral Thesis University of Minnesota, Technical Report, (1997)

[Pe1] Peckham, B. Real Perturbations of Complex Analytic Families: Points to Regions, *International Journal of Bifurcation and Chaos*, Vol. 8, No. 1, (1998), pp. 73-93

[Pe2] Peckham, B. and Montaldi, J. Real Continuation From the Complex Quadratic Family: Fixed-Point Bifurcation Sets, *International Journal of Bifurcation and Chaos*, Vol. 10, No. 2, pp. 391-414, World Scientific Publishing Company, (2000)

[Pe3] Peckham, B. and Bozyk, B. Nonholomorphic Continuations of Holomorphic Families. (in preparation) (2012)